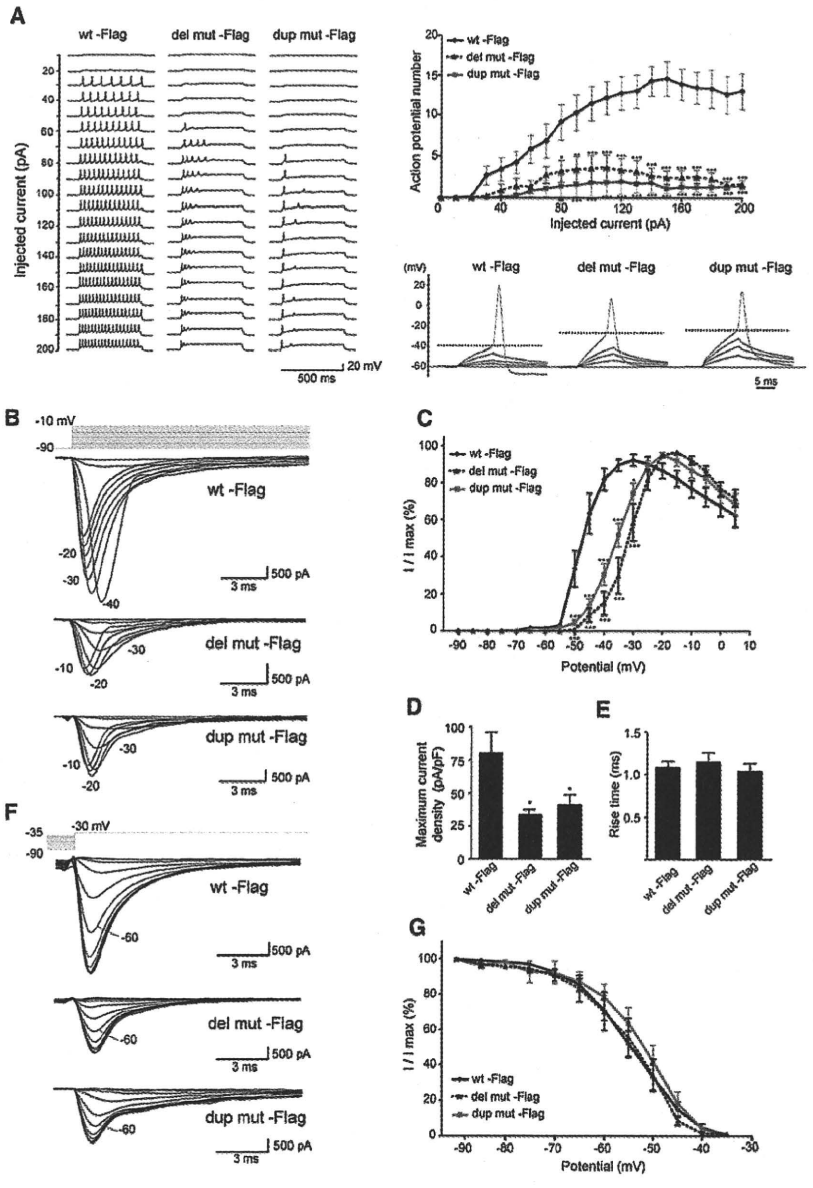


**Figure 6. Mutant α-II Spectrin Elevated Action Potential Threshold in Primary Cultured Cortical Neurons**

(A) Left, representative sets of action potential traces recorded from cultured cortical neurons expressing either WT or mutant α-II spectrin (del mut or dup mut)-Flag-nucEGFP during 500 ms injection of depolarizing current in +10 pA increments, from a holding potential of −60 mV. Right top, input-output relationship of the number of evoked action potentials versus the injected current (WT, n = 7; del mut, n = 9; dup mut, n = 7). Although there were no significant differences in the passive membrane properties among each genotypes (see Table S3), repetitive action potential elicitation was significantly reduced in the two mutants. Right bottom, representative responses to a series of subthreshold and suprathreshold depolarizing current injections of 10 ms duration. A base holding potential (−60 mV) and an identified action potential threshold are indicated by thin and dashed lines, respectively. Note that mutants elevated action potential threshold compared with the WT (see Table S3).

(B–G) Recordings of whole-cell sodium currents with conventional activation (C–E: WT, n = 11; del mut, n = 10; dup mut, n = 10) and inactivation protocols (G: WT, n = 11; del mut, n = 9; dup mut, n = 10).

(B) Representative sets of sodium current traces recorded from dissociated cortical neurons expressing WT and mutant α-II spectrins.

(C) Voltage dependence of channel activation measured during voltage steps between −90 and +10 mV. Statistical analysis indicated that del mut and dup mut exhibited significant differences in current-voltage relationship compared with the WT. Both mutants displayed a significant depolarizing shift in activation compared with the WT.

(D) Peak current density elicited by test pulses. Statistical analysis indicated a significant reduction in peak current in both mutants compared with the WT.

(E) Activation kinetics assessed by 10%–90% rise time plotted against test potential for WT and mutants. There were no significant differences among WT and the two mutants.

(F) Representative sodium currents in neurons expressing WT or mutant α-II spectrin under influence of 500 ms inactivation prepotentials.

(G) Voltage dependence of inactivation assessed in response to inactivating prepulses between −90 and −35 mV. Statistical analysis revealed no significant differences among WT and mutants ($p = 0.96$).

Error bars, SEM. $^{*}p < 0.05$, $^{**}p < 0.01$, $^{***}p < 0.001$, as compared to the WT. Most of the recorded parameters are summarized in Table S3.

group A. Although subject 1 initially showed severe hypomyelination, the myelination showed catch-up completion at 4 years of age. These facts suggest that *SPTAN1* hemizygosity may have temporary effects on the myelination. Further reports of microdeletions involving *SPTAN1* may give us a clear answer about the contribution of *SPTAN1* hemizygosity to hypomyelination. By contrast, subjects 2 and 3 showed more severe phenotypes than subject 1, indicating that the effect of in-frame mutations was dominant negative rather than loss of function. This idea was supported by the fact that the in-frame mutations could cause aggregation of α-II/β-II and α-II/β-III spectrin heterodimers, related to disturbed clustering of ankyrinG and VGSC at AIS. β-II and β-III spectrins have been shown to participate in stabilization of membrane proteins and axonal transport.[25,26] Although our study did not detect aggregation of the α-II/β-IV spectrin heterodimer, which is essential for stabilization of membrane proteins at

AIS,[27,28] defective α-II/β-II and α-II/β-III spectrin heterodimers might affect the stability of membrane proteins at AIS, possibly in combination with disrupting intracellular transport.

The α-II (mut)/β-II spectrin heterodimers was more unstable than the α-II (WT)/β-II heterodimers, which was manifested by CD melting experiments as differences of melting points at relatively high temperature (50°C–60°C and 70°C–80°C). In general, structural instability of proteins would lead to aggregate formation. Immunofluorescence analysis in both transiently transfected primary neuron and LCL derived from two subjects showed aggregation of α-II/β-II and α-II/β-III spectrin heterodimers, suggesting that structual instability of α-II/β-II and α-II/β-III spectrin heterodimers resulted in the aggregation.

We demonstrated a possible link between a mutant submenbranous scaffolding protein and abnormal AIS integrity. It has been suggested that the levels of ion channels at AIS are regulated by altering the cytoskeletal scaffolds.[22] A recessive mutation of scaffolding protein CASPR2 causes focal epilepsy.[29] Abnormal AIS integrity resulting from mutant α-II spectrin further underscores the importance of AIS scaffolds in the pathogenesis of epilepsy and provides new insights for WS.

## Supplemental Data

Supplemental Data include two figures and three tables and can be found with this article online at http://www.cell.com/AJHG.

## Acknowledgments

The authors declare no conflict of interest. We would like to thank all the patients and their families for their participation in this study. We also thank Dr. Jun-ichi Miyazaki for permitting use of CAG promoter and Dr. Sean Megason for the pCIG vector. This work was supported by research grants from the Ministry of Health, Labour, and Welfare (N.M., J.T., and M. Kato), the Japan Science and Technology Agency (N.M.), a Grant-in-Aid for Scientific Research on Priority Areas (Research on Pathomechanisms of Brain disorder) from the Ministry of Education, Culture, Sports, Science, and Technology of Japan (N.M.), a Grant-in-Aid for Scientific Research from Japan Society for the Promotion of Science (N.M. and M. Kato), a Grant-in-Aid for Young Scientist from Japan Society for the Promotion of Science (H.S.), the Research Promotion Fund from Yokohama Foundation for Advancement of Medical Science (H.S.), the Research Promotion Fund from the Uehara Memorial Foundation (H.S.), research grants from the Japan Epilepsy Research Foundation (H.S.), a grant from the 2009 Strategic Research Project of Yokohama City University (H.S.), and a research grant from the Naito Foundation (N.M.). This work has been done at Advanced Medical Research Center, Yokohama City University.

Received: March 11, 2010
Revised: April 29, 2010
Accepted: April 30, 2010
Published online: May 20, 2010

## Web Resources

The URLs for data presented herein are as follows:

ClustalW, http://align.genome.jp/
dbSNP, http://www.ncbi.nlm.nih.gov/projects/SNP/
GenBank, http://www.ncbi.nlm.nih.gov/Genbank/
Online Mendelian Inheritance in Man (OMIM), http://www.ncbi.nlm.nih.gov/Omim/
Phyre, http://www.sbg.bio.ic.ac.uk/phyre/
Protein Data Bank, http://www.pdb.org/pdb/home/home.do
PyMOL, http://www.pymol.org/
UCSC Genome Browser, http://genome.ucsc.edu/cgi-bin/hgGateway

## References

1. Kato, M. (2006). A new paradigm for West syndrome based on molecular and cell biology. Epilepsy Res. *70* (*Suppl 1*), S87–S95.
2. Bahi-Buisson, N., Nectoux, J., Rosas-Vargas, H., Milh, M., Boddaert, N., Girard, B., Cances, C., Ville, D., Afenjar, A., Rio, M., et al. (2008). Key clinical features to identify girls with *CDKL5* mutations. Brain *131*, 2647–2661.
3. Strømme, P., Mangelsdorf, M.E., Shaw, M.A., Lower, K.M., Lewis, S.M., Bruyere, H., Lütcherath, V., Gedeon, A.K., Wallace, R.H., Scheffer, I.E., et al. (2002). Mutations in the human ortholog of *Aristaless* cause X-linked mental retardation and epilepsy. Nat. Genet. *30*, 441–445.
4. Kato, M., Das, S., Petras, K., Sawaishi, Y., and Dobyns, W.B. (2003). Polyalanine expansion of ARX associated with cryptogenic West syndrome. Neurology *61*, 267–276.
5. Djukic, A., Lado, F.A., Shinnar, S., and Moshé, S.L. (2006). Are early myoclonic encephalopathy (EME) and the Ohtahara syndrome (EIEE) independent of each other? Epilepsy Res. *70* (*Suppl 1*), S68–S76.
6. Ohtahara, S., and Yamatogi, Y. (2006). Ohtahara syndrome: With special reference to its developmental aspects for differentiating from early myoclonic encephalopathy. Epilepsy Res. *70* (*Suppl 1*), S58–S67.
7. Saitsu, H., Kato, M., Mizuguchi, T., Hamada, K., Osaka, H., Tohyama, J., Uruno, K., Kumada, S., Nishiyama, K., Nishimura, A., et al. (2008). *De novo* mutations in the gene encoding STXBP1 (MUNC18-1) cause early infantile epileptic encephalopathy. Nat. Genet. *40*, 782–788.
8. Bennett, V., and Healy, J. (2008). Organizing the fluid membrane bilayer: Diseases linked to spectrin and ankyrin. Trends Mol. Med. *14*, 28–36.
9. Bennett, V., and Baines, A.J. (2001). Spectrin and ankyrin-based pathways: Metazoan inventions for integrating cells into tissues. Physiol. Rev. *81*, 1353–1392.
10. Ikeda, Y., Dick, K.A., Weatherspoon, M.R., Gincel, D., Armbrust, K.R., Dalton, J.C., Stevanin, G., Dürr, A., Zühlke, C., Bürk, K., et al. (2006). Spectrin mutations cause spinocerebellar ataxia type 5. Nat. Genet. *38*, 184–190.
11. Perrotta, S., Gallagher, P.G., and Mohandas, N. (2008). Hereditary spherocytosis. Lancet *372*, 1411–1426.
12. Meary, F., Metral, S., Ferreira, C., Eladari, D., Colin, Y., Lecomte, M.-C., and Nicolas, G. (2007). A mutant alphaII-spectrin designed to resist calpain and caspase cleavage questions the functional importance of this process in vivo. J. Biol. Chem. *282*, 14226–14237.

13. Voas, M.G., Lyons, D.A., Naylor, S.G., Arana, N., Rasband, M.N., and Talbot, W.S. (2007). alphaII-spectrin is essential for assembly of the nodes of Ranvier in myelinated axons. Curr. Biol. *17*, 562–568.
14. Tohyama, J., Akasaka, N., Osaka, H., Maegaki, Y., Kato, M., Saito, N., Yamashita, S., and Ohno, K. (2008). Early onset West syndrome with cerebral hypomyelination and reduced cerebral white matter. Brain Dev. *30*, 349–355.
15. Megason, S.G., and McMahon, A.P. (2002). A mitogen gradient of dorsal midline Wnts organizes growth in the CNS. Development *129*, 2087–2098.
16. Niwa, H., Yamamura, K., and Miyazaki, J. (1991). Efficient selection for high-expression transfectants with a novel eukaryotic vector. Gene *108*, 193–199.
17. Kelley, L.A., and Sternberg, M.J. (2009). Protein structure prediction on the Web: A case study using the Phyre server. Nat. Protoc. *4*, 363–371.
18. Kusunoki, H., Minasov, G., Macdonald, R.I., and Mondragón, A. (2004). Independent movement, dimerization and stability of tandem repeats of chicken brain α-spectrin. J. Mol. Biol. *344*, 495–511.
19. Speicher, D.W., Weglarz, L., and DeSilva, T.M. (1992). Properties of human red cell spectrin heterodimer (side-to-side) assembly and identification of an essential nucleation site. J. Biol. Chem. *267*, 14775–14782.
20. Riederer, B.M., Zagon, I.S., and Goodman, S.R. (1986). Brain spectrin(240/235) and brain spectrin(240/235E): Two distinct spectrin subtypes with different locations within mammalian neural cells. J. Cell Biol. *102*, 2088–2097.
21. Xu, J., Ziemnicka, D., Scalia, J., and Kotula, L. (2001). Monoclonal antibodies to alphaI spectrin Src homology 3 domain associate with macropinocytic vesicles in nonerythroid cells. Brain Res. *898*, 171–177.
22. Ogawa, Y., and Rasband, M.N. (2008). The functional organization and assembly of the axon initial segment. Curr. Opin. Neurobiol. *18*, 307–313.
23. Lai, H.C., and Jan, L.Y. (2006). The distribution and targeting of neuronal voltage-gated ion channels. Nat. Rev. Neurosci. *7*, 548–562.
24. Kuba, H., Ishii, T.M., and Ohmori, H. (2006). Axonal site of spike initiation enhances auditory coincidence detection. Nature *444*, 1069–1072.
25. Muresan, V., Stankewich, M.C., Steffen, W., Morrow, J.S., Holzbaur, E.L., and Schnapp, B.J. (2001). Dynactin-dependent, dynein-driven vesicle transport in the absence of membrane proteins: a role for spectrin and acidic phospholipids. Mol. Cell *7*, 173–183.
26. Kizhatil, K., Yoon, W., Mohler, P.J., Davis, L.H., Hoffman, J.A., and Bennett, V. (2007). Ankyrin-G and β2-spectrin collaborate in biogenesis of lateral membrane of human bronchial epithelial cells. J. Biol. Chem. *282*, 2029–2037.
27. Komada, M., and Soriano, P. (2002). [β]IV-spectrin regulates sodium channel clustering through ankyrin-G at axon initial segments and nodes of Ranvier. J. Cell Biol. *156*, 337–348.
28. Parkinson, N.J., Olsson, C.L., Hallows, J.L., McKee-Johnson, J., Keogh, B.P., Noben-Trauth, K., Kujawa, S.G., and Tempel, B.L. (2001). Mutant β-spectrin 4 causes auditory and motor neuropathies in quivering mice. Nat. Genet. *29*, 61–65.
29. Strauss, K.A., Puffenberger, E.G., Huentelman, M.J., Gottlieb, S., Dobrin, S.E., Parod, J.M., Stephan, D.A., and Morton, D.H. (2006). Recessive symptomatic focal epilepsy and mutant contactin-associated protein-like 2. N. Engl. J. Med. *354*, 1370–1377.

*Epilepsia*, 51(12):2397–2405, 2010
doi: 10.1111/j.1528-1167.2010.02728.x

FULL-LENGTH ORIGINAL RESEARCH

# *STXBP1* mutations in early infantile epileptic encephalopathy with suppression-burst pattern

*[1]Hirotomo Saitsu, †[1]Mitsuhiro Kato, *Ippei Okada, ‡Kenji E. Orii, §Tsukasa Higuchi, ¶Hideki Hoshino, ¶Masaya Kubota, #Hiroshi Arai, **Tetsuzo Tagawa, ††Shigeru Kimura, ‡‡Akira Sudo, §§Sahoko Miyama, ¶¶Yuichi Takami, ##Toshihide Watanabe, *Akira Nishimura, *Kiyomi Nishiyama, *Noriko Miyake, ***Takahito Wada, ***Hitoshi Osaka, ‡Naomi Kondo, †Kiyoshi Hayasaka, and *Naomichi Matsumoto

*Department of Human Genetics, Yokohama City University Graduate School of Medicine, Yokohama, Japan; †Department of Pediatrics, Yamagata University Faculty of Medicine, Yamagata, Japan; ‡Department of Pediatrics, Graduate School of Medicine, Gifu University, Gifu, Japan; §Department of Pediatrics, Shinshu University School of Medicine, Matsumoto, Japan; ¶Division of Neurology, National Center for Child Health and Development, Tokyo, Japan; #Department of Pediatric Neurology, Morinomiya Hospital, Osaka, Japan; **Department of Pediatrics, Osaka Koseinenkin Hospital, Osaka, Japan; ††Department of Pediatrics, Akita Red Cross Hospital, Akita, Japan; ‡‡Department of Pediatrics, Sapporo City General Hospital, Hokkaido, Japan; §§Department of Neurology, Tokyo Metropolitan Children's Medical Center, Fuchu, Japan; ¶¶Department of Pediatrics, Himeji Red Cross Hospital, Himeji, Hyogo, Japan; ##Department of Pediatrics, Hokkaido Medical Center for Child Health and Rehabilitation, Hokkaido, Japan; and ***Division of Neurology, Clinical Research Institute, Kanagawa Children's Medical Center, Yokohama, Japan

## Summary

**Purpose:** De novo *STXBP1* mutations have been found in individuals with early infantile epileptic encephalopathy with suppression-burst pattern (EIEE). Our aim was to delineate the clinical spectrum of subjects with *STXBP1* mutations, and to examine their biologic aspects.

**Methods:** *STXBP1* was analyzed in 29 and 54 cases of cryptogenic EIEE and West syndrome, respectively, as a second cohort. RNA splicing was analyzed in lymphoblastoid cells from a subject harboring a c.663 + 5G>A mutation. Expression of STXBP1 protein with missense mutations was examined in neuroblastoma2A cells.

**Results:** A total of seven novel *STXBP1* mutations were found in nine EIEE cases, but not in West syndrome. The mutations include two frameshift mutations, three nonsense mutations, a splicing mutation, and a recurrent missense mutation in three unrelated cases. Including our previous data, 10 of 14 individuals (71%) with *STXBP1* aberrations had the onset of spasms after 1 month, suggesting relatively later onset of epileptic spasms. Nonsense-mediated mRNA decay associated with abnormal splicing was demonstrated. Transient expression revealed that STXBP1 proteins with missense mutations resulted in degradation in neuroblastoma2A cells.

**Discussion:** Collectively, *STXBP1* aberrations can account for about one-third individuals with EIEE (14 of 43). These genetic and biologic data clearly showed that haploinsufficiency of *STXBP1* is the important cause for cryptogenic EIEE.

**KEY WORDS:** *STXBP1*, EIEE, West syndrome, Haploinsufficiency.

Early infantile epileptic encephalopathy with suppression-burst (EIEE), also known as Ohtahara syndrome (Ohtahara et al., 1976), is characterized by early onset of tonic seizures, seizure intractability, characteristic suppression-burst patterns on electroencephalography (EEG), and poor outcome with severe psychomotor retardation (Djukic et al., 2006; Ohtahara & Yamatogi, 2006). We recently found de novo mutations in *STXBP1* (encoding syntaxin binding protein 1, also known as MUNC18-1) in individuals with EIEE (Saitsu et al., 2008). The subjects with *STXBP1* aberrations, including four missense mutations and a 2-Mb microdeletion encompassing *STXBP1*, showed the characteristic feature of EIEE. A mutant protein with a missense change (p.C180Y) showed structural instability with significant thermolability and impaired binding to syntaxin-1A compared with the wild-type (Saitsu et al., 2008). These findings suggest that haploinsufficiency of *STXBP1* causes EIEE.

Accepted August 4, 2010; Early View publication September 30, 2010.
Address correspondence to Dr. Hirotomo Saitsu, Department of Human Genetics, Yokohama City University Graduate School of Medicine, 3-9 Fukuura, Kanazawa-ku, Yokohama 236-0004, Japan. E-mail: hsaitsu@yokohama-cu.ac.jp
[1]These authors contributed equally to this work.

West syndrome is one of the most common infantile epileptic syndromes and is characterized by epileptic spasms, arrest of psychomotor development, and hypsarrhythmia on EEG (Kato, 2006). Brain malformations and metabolic disorders were found as underlying causes of symptomatic West syndrome, but many cryptogenic cases remain etiologically unexplained (Kato, 2006). Two causative genes, *ARX* (aristaless related homeobox) and *CDKL5* (cyclin-dependent kinase-like 5), are mutated only in a subset of familial and sporadic cases of West syndrome (Stromme et al., 2002; Kalscheuer et al., 2003; Kato et al., 2003; Weaving et al., 2004; Guerrini et al., 2007; Bahi-Buisson et al., 2008). EIEE and West syndrome are considered as a continuum of epileptic encephalopathies because the majority (75%) of EIEE transit to West syndrome (Yamatogi & Ohtahara, 2002; Ohtahara & Yamatogi, 2006). Specific mutations of *ARX* have been also found in EIEE (Kato et al., 2007), further suggesting a common pathologic mechanism among two syndromes. *STXBP1* mutations would be possibly involved in West syndrome. However, it remains to be determined.

To delineate the clinical spectrum of *STXBP1* mutations, a second cohort consisting of EIEE and West syndrome cases was investigated. Novel *STXBP1* mutations have been found only in EIEE cases. We also characterized biologic aspects of *STXBP1* mutations by using lymphoblastoid cells derived from a patient, and by transient expression of mutant STXBP1 proteins in neuroblastoma2A cells.

## Subjects and Methods

### Subjects

A total of 29 and 54 Japanese individuals with EIEE and West syndrome, respectively, were newly recruited as a second cohort. Brain malformations were not found in all cases. The diagnosis was made on the basis of clinical features and characteristic patterns on EEG. Experimental protocols were approved by Institutional Review Boards for Ethical Issues at Yokohama City University School of Medicine and Yamagata University Faculty of Medicine. Informed consent was obtained from all individuals and/or their families in agreement with the requirements of Japanese regulations. Clinical aspects of subjects with *STXBP1* mutations are summarized in Table 1.

### Mutation screening

Genomic DNA was obtained from peripheral blood leukocytes according to standard protocols. Mutation screening of 1st to 20th exons covering the coding region of *STXBP1* was performed by high-resolution melt analysis (HRM). Realtime polymerase chain reaction (PCR) and HRM were serially performed in a 12-$\mu$l mixture on RotorGene-6200 HRM (Corbett Life Science, Brisbane, Qld, Australia). For the 2nd to 20th exons, PCR mixture contained 1× ExTaq buffer, 0.2 mM each dNTP, 0.25 $\mu$M each primer, 1.5 $\mu$M SYTO9 (Invitrogen, Carlsbad, CA, U.S.A.), and 0.375 U Ex TaqHS polymerase (Takara Bio, Ohtsu, Japan). For the first exon, the PCR mixture contains 1× PCR Buffer for KOD FX, 0.4 mM each dNTP, 0.3 $\mu$M each primer, 1.5 $\mu$M SYTO9, and 0.3 U KOD FX polymerase (Toyobo, Osaka, Japan). PCR primers and conditions are shown in Table S1. PCR samples showing an aberrant melting curve pattern were sequenced as previously described (Saitsu et al., 2008). For all the families showing de novo mutations, parentage was confirmed by microsatellite analysis as described previously (Saitsu et al., 2008).

### RNA analysis

Lymphoblastoid cells (LCL) derived from a subject harboring a c.663 + 5G>A mutation was grown in Roswell Park Memorial Institute 1,640 medium supplemented with 10% fetal bovine serum (FBS), 1× Antibiotic-Antimycotic (Invitrogen), and 8 $\mu$g/ml tylosin (Sigma, Tokyo, Japan) at 37°C in a 5% $CO_2$ incubator. After incubation with dimethyl sulfoxide (DMSO) (as vehicle control) or 30 $\mu$M cycloheximide (Sigma) for 4 h, total RNA was extracted using TRizol (Invitrogen). One $\mu$g total RNA was subjected to reverse transcription using PrimeScript 1st strand synthesis kit with random hexamers (Takara). Minus reverse transcriptase (RT) control with no reverse transcriptase was included in each experiment. PCR was performed in a 15-$\mu$l mixture, containing 1 $\mu$l cDNA, 1× PCR Buffer for KOD FX, 0.4 mM each dNTP, 0.3 $\mu$M each primer, and 0.3 U KOD FX polymerase (Toyobo). Primer sequences are 5′-CTTTGTGCCACCCTGAAGGAGTACC-3′ in ex7-F and 5′-CAGTGCTATCCACAGGTCGTCGTC-3′ in ex10-R. The control cDNA isolated from a normal LCL sample was used as a reference. PCR products electrophoresed in 2% agarose gel were stained with ethidium bromide, and were analyzed by quantitative densitometry on FluorChem 8,900 (Alpha Innotech, San Leandro, CA, U.S.A.). Experiments were repeated three times. Inhibition of nonsense-mediated mRNA decay (NMD) was estimated according to the density ratios of upper normal and lower aberrant bands with/without 30 $\mu$M cyclophosphamide treatment in the culture of the patient's LCL. Statistical analyses were done using the unpaired Student's *t*-test (two-tailed). Each PCR band was sequenced using purified DNA by QIAEXII Gel extraction kit (Qiagen, Tokyo, Japan).

### Expression vectors

A fragment containing internal ribosomal entry signal (IRES) and nuclear-localized Flag-DsRed was inserted into pEGFP-C1 vector (Clontech, Mountain View, CA, U.S.A.). Human *STXBP1* cDNA was fused to this vector, achieving dual expression of both N terminal EGFP-tagged STXBP1 and nuclear-localized Flag-DsRed. A wild-type *STXBP1* cDNA, four mutants (c.251T>A, p.V84D; c.539G>A, p.C180Y; c.1328T>G, p.M443R; c.1631G>A, p.G544D) and two normal variants (c.250G>A, p.V84I; c.1292A>T,

**Table 1. Summary of clinical features of subjects with *STXBP1* mutations**

| Subject (age) | Sex | Mutation | Dx | Age at onset | Initial symptoms | Initial EEG | Age at onset of spasms | Age at onset of SB pattern | Age at transit to WS | Transition from spasms to other seizures | Transition to other EEG findings | Response to therapy | Development | Neurologic examination | Magnetic resonance imaging |
|---|---|---|---|---|---|---|---|---|---|---|---|---|---|---|---|
| 1,751 (3 y) | M | c.1217G>A p.R406H de novo | EIEE | 0 d | Bilateral convulsion | SB | 3 w | 1 m | 5 m | No | Multifocal spike and slow wave complex | Intractable, hourly | No head control, No social contact | Profound MR, Severe spastic quadriplegia | Normal at 1 m, Mild brain atrophy at 3 y |
| 1,989 (15 m) | M | c.1217G>A p.R406H *de novo* | EIEE | 43 d | GTCS with upward eye gazing | SB | 2 m | 1 m | 2 m | ~48 d myoclonic seizure | No | Intractable, daily | No head control, No social contact | Profound MR, Severe spastic quadriplegia | Normal at 11 m |
| 2,123 (20 m) | M | c.1217G>A p.R406H *de novo* | EIEE | 15 d | Partial seizures (right hemiconvulsion) | Focal spike at P3 | 2 m | 2 m | No | Tonic seizure to myoclonic seizure | Unknown | Intractable, daily | No head control, No social contact | Profound MR, Severe spastic quadriplegia | Normal at 1 m, Mild frontal brain atrophy at 20 m |
| 1,792 (6 y) | F | c.157G>T p.E53X *de novo* | EIEE | 2 d | Spasms | SB | 2 d | 1 w | 6 m | Versive seizure after hypoxia at 2 y | Multifocal irregular spikes | Intractable, daily | No head control, No social contact | Profound MR, Severe spastic quadriplegia | Normal at 0 m, Mild ventricular dilatation at 14 m |
| 1,694 (17 m) | M | c.388_389delCT p.L130DfsX11 *de novo* | EIEE | 2 m | Secondary generalized seizures initiated from the right face | SB with fluctuated baseline | 2 m | 2 m | 3 m | CPS | Multifocal spike and slow wave complex with desynchronization | Seizure-free after ACTH or VPA with KBr | No head control, No social contact | Profound MR, Severe spastic quadriplegia | Normal at 3 m |
| 1,951 (6 m) | F | c.663 + 5G>A *de novo* | EIEE | 5 d | Blinking to tonic seizures | SB with fluctuated baseline | 1 m | 1 m | 3 m | Tonic seizure | Left temporal spike and slow wave complex | Seizure free with VB6 for spasms and ACTH for WS | Eye pursuit and smiling from 4 m, Head control and rolling over from 6 m | Moderate MR, Quadriplegia | Normal at 0 m, subdural effusion at 2 m |
| 1,655 (6 m) | M | c.703C>T p.R235X *de novo* | EIEE | 1 m | Spasms in cluster | SB | 1 m | 1 m | No | No | Occipital spikes | Seizure free from 6 m after high-dose PB | No head control, No social contact | Profound MR, Severe spastic quadriplegia | Delayed myelination and brain atrophy |
| 2,103 (11 m) | F | c.747dupT p.Q250SfsX6 *de novo* | EIEE | 3 d | Clonic convulsion | Focal spike at C3, Cz, Fz | 31 d | 1 m | 10 m | Partial seizure (abnormal eye movement) and myoclonic seizures | Multifocal spikes | Intractable, hourly | No head control, Smiling from 5 m | Profound MR, Severe spastic quadriplegia | Normal at 1 m, left mild brain atrophy at 3 m |
| 1,979 (10 y) | M | c.961A>T p.K321X *de novo* | EIEE | 2 w | Partial seizures | SB | 3 w | 1 m | 3 m | Partial seizure | Multifocal spikes with asymmetric background activity | Intractable, daily | No head control, No social contact | Profound MR, Severe spastic quadriplegia | Normal at 0 m, Brain atrophy and subdural hematoma at 7 m after ACTH |

Dx, diagnosis; GTCS, generalized tonic–clonic seizures; SB, suppression-burst; WS, West syndrome; CPS, complex partial seizure; ACTH, adrenocorticotropic hormone; VPA, valproic acid; KBr, potassium bromide; VB6, vitamin $B_6$; PB, phenobarbital; MR, mental retardation; d, day(s); w, week; m, month(s); y, year(s); 0 w, 0–6 days; 0 m, 0–3 week.



*Epilepsia*, 51(12):2397–2405, 2010
doi: 10.1111/j.1528-1167.2010.02728.x

p.Q431L) were generated as described previously (Saitsu et al., 2008). c.250G>A was registered as single nucleotide polymorphism (SNP) (rs34830702). c.1292A>T was observed in one of 250 normal controls (allele frequency: 1/500), but not in EIEE or West syndrome.

**Cell culture, transfection, and immunoblotting**

Mouse neuroblastoma 2A (N2A) cells were grown as described previously (Saitsu et al., 2008). For transient expression experiments, N2A cells on glass cover slips (in 24-well plates for microscopic detection) and 3.5-cm culture dish (for immunoblotting) were transfected with 200 and 800 ng of plasmid DNA using FuGene6 reagent (Roche diagnostics, Tokyo, Japan), respectively. After 3 h, culture medium was changed to low serum medium (5% FBS) with 20 $\mu$M all transretinoic acid (Sigma) in order to induce neural differentiation, and cells were subsequently cultured for 2 days. For microscopic detection, N2A cells were washed in phosphate-buffered saline (PBS) and fixed in 4% paraformaldehyde/PBS for 15 min. Cover slips were mounted using Vectashield with DAPI (Vector Laboratories, Youngstown, OH, U.S.A.) and images were visualized with an AxioCam MR CCD fitted to Axioplan2 fluorescence microscope (Carl Zeiss, Tokyo, Japan), and captured using Axio Vision 4.5 software (Carl Zeiss). The exposure time for enhanced green fluorescent protein (EGFP) and DsRed capture was fixed in a series of experiments to enable direct comparison between different experimental samples. For immunoblotting, N2A cells were washed twice in ice-cold PBS, and lysed in sodium dodecyl sulfate (SDS) sample buffer. Samples were size-fractionated by sodium dodecyl sulfate-polyacrylamide gel electrophoresis (SDS-PAGE), transferred to the polyvinylidene difluoride (PVDF) membrane, and analyzed with anti-Munc18 (for STXBP1 detection, 1:5,000 dilution) (BD Transduction Laboratories, Tokyo, Japan) or anti-Flag M2 (1:2,000 dilution) (Sigma) antibody. Secondary antibody was peroxidase-conjugated goat anti-mouse IgG (Jackson ImmunoResearch, West Grove, PA, U.S.A.). Blots were detected using the Supersignal West dura (Pierce, Yokohama, Japan). Chemiluminescence was evaluated by quantitative densitometry using a FluorChem 8,900 (Alpha Innotech). Experiments were repeated three times.

## Results

A total of seven novel heterozygous mutations found in six males and three females are presented together with four reported missense mutations in Fig. 1 (Saitsu et al., 2008). The recurrent p.R406H mutation occurred at evolutionary conserved amino acid (Fig. 1). All the mutations are novel and occurred de novo. Parentage was confirmed using several microsatellite markers (data not shown). All the mutations were found only in EIEE cases, but not in West syndrome.

**Clinical features of *STXBP1* aberrations**

Detailed clinical information of individuals with *STXBP1* mutations is summarized in Table 1. All nine individuals were born at term without asphyxia except for the subject 1,751 who had the short umbilical cord. Their body weight, height, and head circumference were normal at birth other than the subject 1,792 with mild microcephaly [30.5 cm, −2.0 standard deviation (SD)]. Epileptic spasms were preceded by other seizure types including partial seizures in seven subjects (other than 1,792 and 1,655), and initial EEG in two subjects showed focal epileptic discharges (2,123 and 2,103). Only one subject demonstrated suppression-burst pattern on EEG (Fig. 2A) in the neonatal period. Transition to West syndrome was observed in seven subjects with EIEE. Although seizures were intractable in six subjects, three subjects responded to medication, such as adrenocorticotropic hormone (ACTH) injection, vitamin $B_6$, high-dose phenobarbital, and valproic acid. All subjects demonstrated severe psychomotor developmental delay, and only two subjects had the social smile. Most subjects presented with normal brain at the first magnetic resonance imaging (MRI), and then showed mild brain atrophy, which might be influenced by ACTH injection, after 1 year (Fig. 2B).

**Abnormal splicing and nonsense-mediated mRNA decay**

To observe mutational effects of c.663 + 5G>A (intron 8), reverse transcriptase PCR was performed using total RNA extracted from LCL derived from the subject 1,951. PCR primers were designed to amplify exons 7 to 10 (Fig. 3A). Only one band (338 bp), corresponding to the wild-type *STXBP1* allele, was amplified using a cDNA template from a control LCL (Fig. 3B). In contrast, a smaller band was detected from the subject's cDNA (Fig. 3B). Direct sequencing of both fragments revealed that exon 8 was skipped in the abnormal band (Fig. 3B), resulting in the insertion of nine new amino acids followed by a premature stop codon at position 203. As intensity of the smaller band was significantly weak (Fig. 3B), NMD may be involved (Maquat et al., 1981; Shyu et al., 2008). Intensity ratio of mutant versus normal band was 29% in untreated condition. The ratio was raised up to 67% after 30-$\mu$M cycloheximide treatment preventing NMD (Fig. 3C), suggesting that the early truncated mutant mRNA underwent degradation by NMD.

**Degradation of mutant STXBP1 proteins**

We previously demonstrated that intense fluorescence signals in clusters likely representing protein aggregation were observed in approximately 20% of N2A cells transiently expressing mutant EGFP-STXBP1 (p.V84D, p.C180Y, p.M443R, and p.G544D), suggesting structural instability of STXBP1 proteins with missense mutations (Saitsu et al., 2008). The other 80% of cells showed diffuse

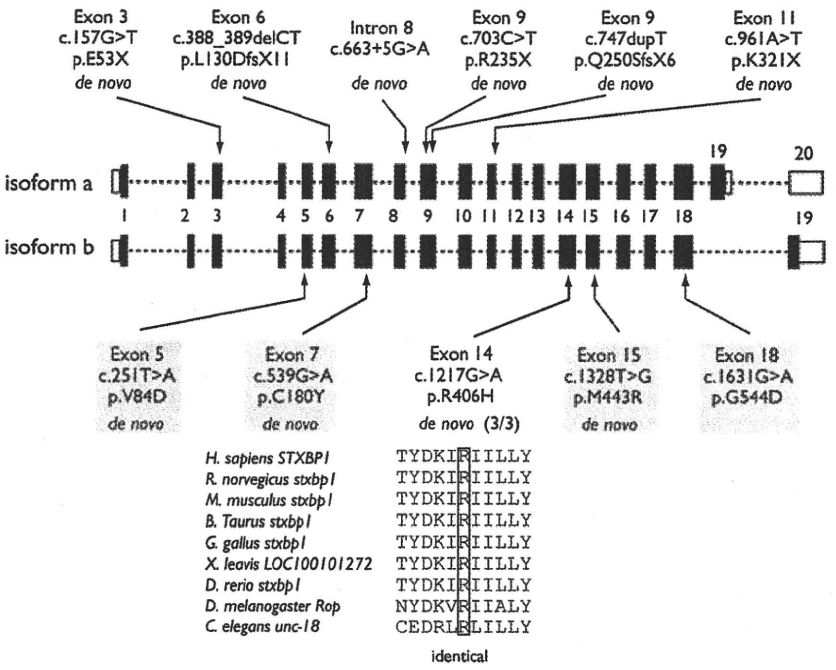


**Figure 1.**

Summary of *STXBP1* mutations found in Japanese individuals with EIEE. Schematic representation of *STXBP1* consisting of at most 20 exons (untranslated region and coding region are open and filled rectangles, respectively). There are two isoforms, a (GenBank accession number, NM_003165) with exon 19, and b (NM_001032221) without exon 19 of isoform a. The location of mutations is indicated by arrows. A total of 11 different mutations were presented: missense mutations below the gene scheme and the other types of mutations above the gene. Four mutations previously reported are in shadow (Saitsu et al., 2008), and seven without shadow are newly found in this study. All the seven novel mutations occurred de novo. The recurrent p.R406H missense mutation found in three unrelated subjects occurred at evolutionary conserved amino acids. CLUSTALW website (http://align.genome.jp/) was used to align homologs of different species.



cytosolic protein distribution similar to that expressing the wild-type, but the signal intensity was much weaker, implying possible protein degradation. To observe mutant protein degradation, a dual-expression vector of EGFP-STXBP1 and nuclear Flag-DsRed (EGFP-STXBP1-IRES-nuclear Flag-DsRed) was generated. Two days after transfection, the wild-type EGFP-STXBP1 was expressed in cytosol, but not in nucleus or plasma membrane as described previously (Saitsu et al., 2008). Notably, in mutant EGFP-STXBP1 transfected cells (p.V84D, p.C180Y, p.M443R, and p.G544D), EGFP signals were almost absent, whereas nuclear DsRed was expressed at comparable levels to that of wild-type (Fig. 4A). Two normal variants, p.V84I and p.Q431L, were expressed in a manner similar to that of the wild-type, with less intensity for a p.Q431L variant (Fig. 4A). Decreased level of mutant STXBP1 expression was confirmed by immunoblotting using Munc18 antibody (Fig. 4B, top). Transfection efficacy or amount of protein loading was similar in all cases based on the level of Flag-DsRed (Fig. 4B, bottom).

## Discussion

We could successfully find a total of seven novel mutations: two frameshift mutations (2-bp deletion and 1-bp insertion), three nonsense mutations, a splicing mutation, and a recurrent missense mutation. Transcripts associated with frameshift, nonsense, and splicing mutations are likely to be degraded by NMD. In the case harboring c.663 + 5G>A, aberrant splicing associated with NMD was demonstrated in LCL derived from the subject. Moreover, mutated STXBP1 proteins underwent degradation in N2A cells. Variable expression of mutated STXBP1 proteins has been also reported in HeLa cells (Ciufo et al., 2005), suggesting that degradation mechanism of mutated STXBP1 proteins may be common in mammalian cells. Considering these genetic and biologic data presented here as well as a complete deletion of *STXBP1* in one EIEE case (Saitsu et al., 2008), haploinsufficiency of *STXBP1* consistently results in EIEE.

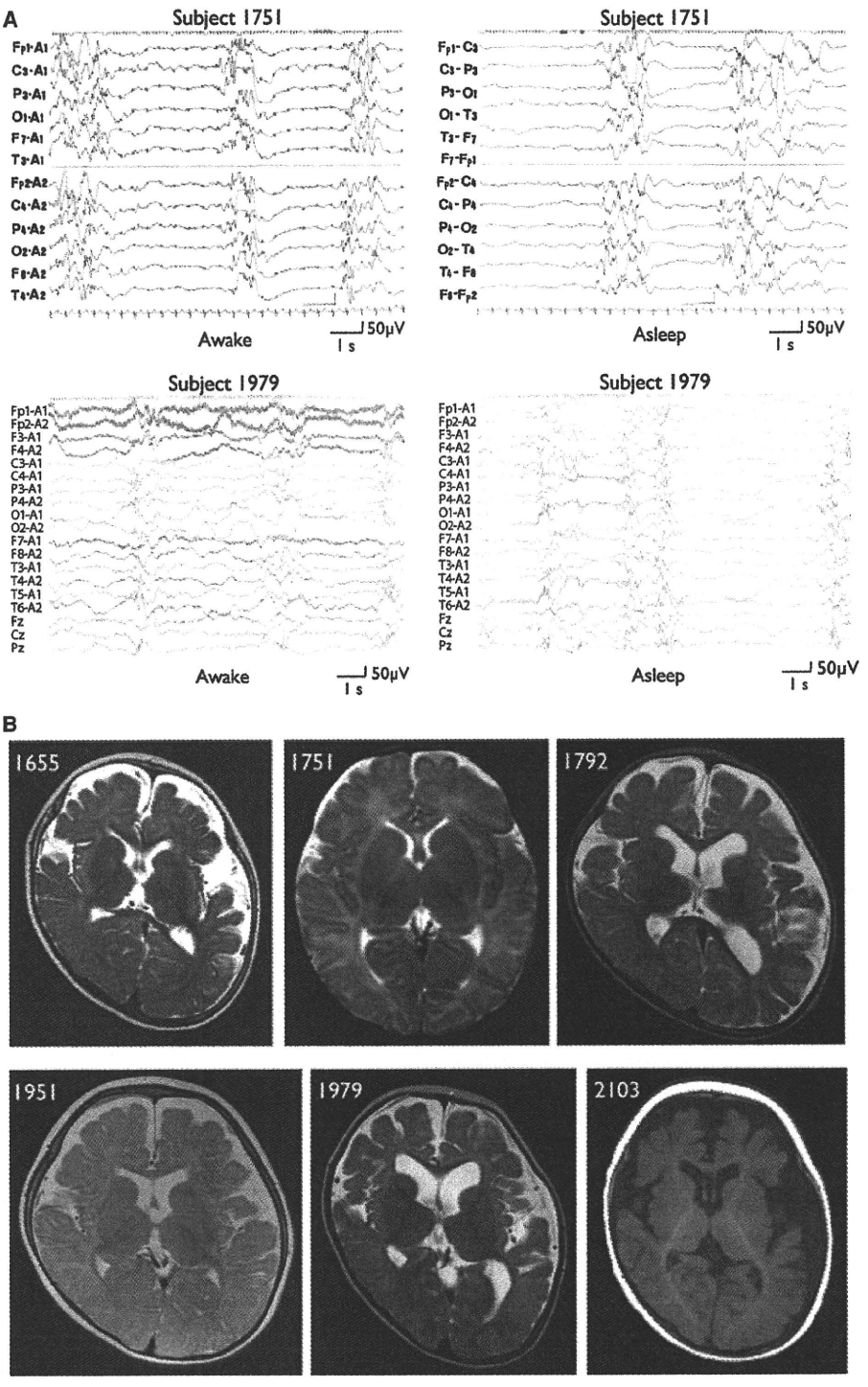


**Figure 2.**
EEG and brain MRI of subjects with *STXBP1* mutations. (**A**) EEG of subjects 1,751 and 1,979 at 1 month of age. Suppression-burst pattern characterized by diffuse bursts of irregular spikes and slow waves lasting 1 to 3 s with low-amplitude background lasting 2–5 s are seen during both sleep and wake. (**B**) $T_2$-weighted brain MRI scan of subjects 1,655 at 9 months of age, 1,751 at 1 month, 1,792 at 15 months, 1,951 at 1 month, and 1,979 at 15 months, and $T_1$-weighted MRI scan of subject 2,103 at 5 months. Mild dilation of lateral ventricles is seen in patients with 1,792, 1,951, 1,979, and 2,103, but none shows brain malformation.


*Epilepsia*, 51(12):2397–2405, 2010
doi: 10.1111/j.1528-1167.2010.02728.x

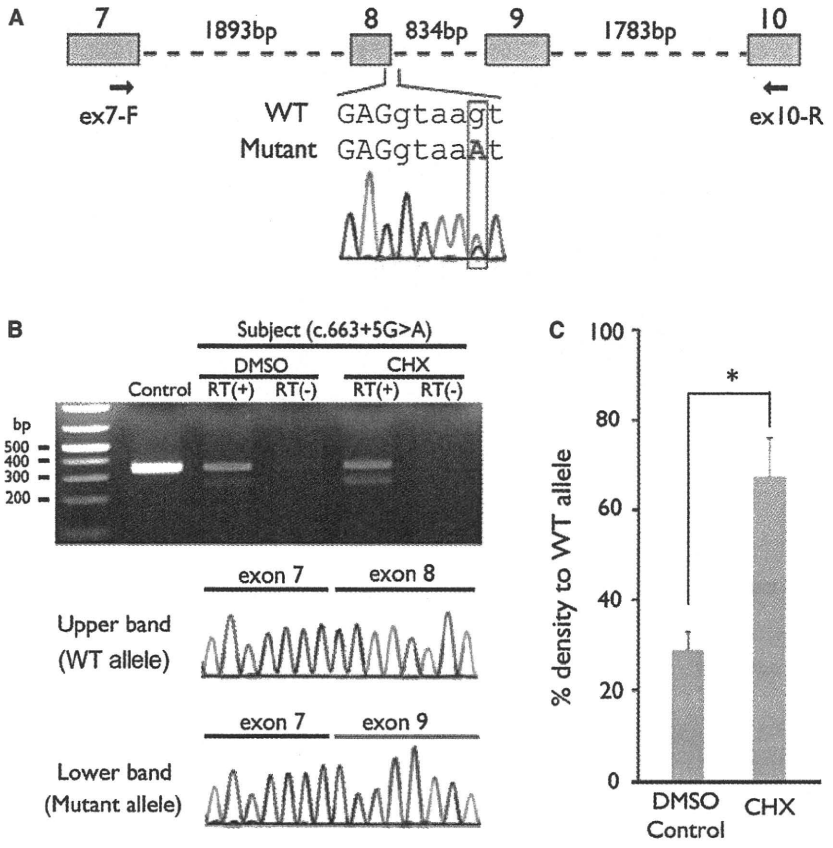


**Figure 3.**
The c.663 + 5G>A mutation causing abnormal splicing associated with NMD. (**A**) Schematic representation of the genomic structure from exons 7–10 of *STXBP1*. Exons, introns, and primers are shown by boxes, dashed lines, and arrows, respectively. The mutation in intron 8 was colored in red. Sequences of exon and intron are presented in upper and lower cases, respectively. (**B**) RT-PCR analysis of subject 1,951 with c.663 + 5G>A and a normal control. Two PCR products were detected from the subject's cDNA: upper was the wild-type (WT) transcript and lower was the mutant. Only a single WT amplicon was detected in a control. The mutant amplicon was significantly increased by 30 $\mu$M cycloheximide (CHX) treatment compared to DMSO treatment as a vehicle control. RT (+): with reverse transcriptase, RT (−): without reverse transcriptase as a negative control. Sequence of WT and mutant amplicons clearly showed exon 8 skipping in the mutant allele. (**C**) Quantitative analysis of the NMD inhibition by CHX based on the data shown in (**B**). *p = 0.0023 by unpaired Student's *t*-test, two tailed. Averages of three repeated experiments are shown with error bars (SD).


The subjects with *STXBP1* mutations in this study showed distinctive features of EIEE, such as early onset seizures, typically frequent epileptic spasms, suppression-burst pattern on EEG, transition to West syndrome after a few to several months, and severe developmental delay, as described in our previous report (Saitsu et al., 2008). Taken together, 14 individuals with EIEE have been found to be associated with *STXBP1* aberrations. A detailed analysis of clinical features revealed that the age at onset of epileptic spasms is rather later in subjects with *STXBP1* aberrations compared to the 16 original subjects reported by Yamatogi and Ohtahara (2002). Only 29% of the subjects (4 of 14) in our series had the onset of spasms within 1 month in contrast to 75% (12 of 16) in the series of Yamatogi and Ohtahara (2002). Although the subjects with *STXBP1* aberrations should be diagnosed as EIEE, the late onset of spasms would suggest that *STXBP1* aberrations could cause an intermediate epileptic encephalopathy between EIEE and West syndrome. The presence of two subjects showing suppression-burst pattern with fluctuated baseline, which could be regarded as intermediate pattern between suppression-burst and hypsarrhythmia, may support this idea.

Another interesting feature is the presence of myoclonic seizures, which are thought to be rather rarely observed in EIEE cases, in three subjects with *STXBP1* mutations (1,989, 2,123, and 2,103). Myoclonic seizures are the main ictal symptom of early myoclonic encephalopathy (EME), which is another epileptic syndrome showing suppression-burst patterns on EEG (Engel, 2006). The prevailing initial seizure type is a main difference between EIEE and EME:

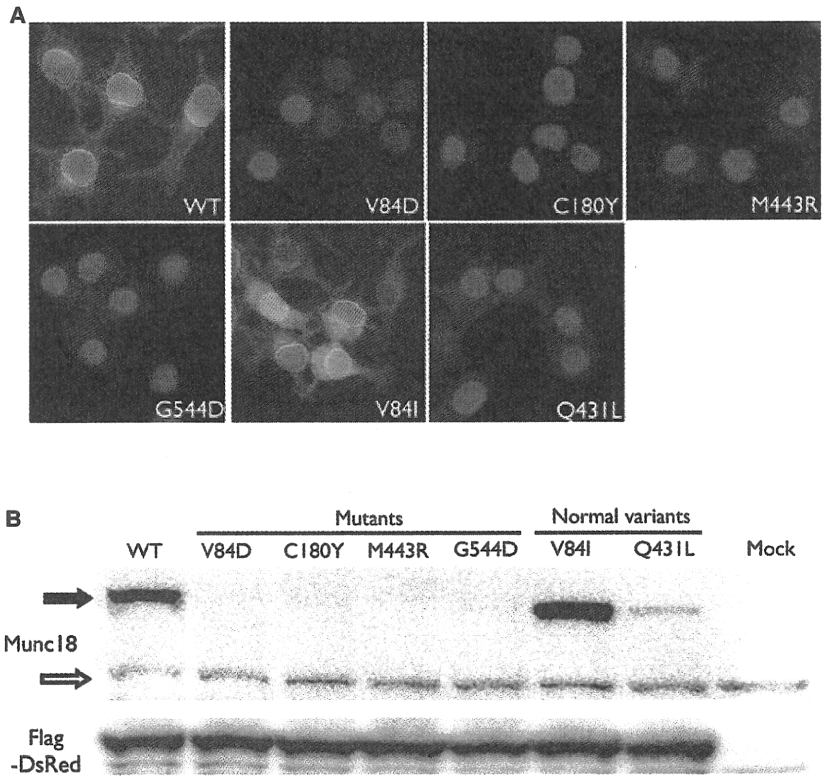


**Figure 4.**
Degradation of mutant EGFP-STXBP1 proteins in N2A cells. (**A**) The wild-type (WT) EGFP-STXBP1 was expressed in cytosol, but not in nucleus or in plasma membrane. In contrast, cells transfected with mutant EGFP-STXBP1 (p.V84D, p.C180Y, p.M443R, and p.G544D) showed almost absent EGFP signals, whereas nuclear DsRed was expressed at levels comparable to that of WT. The p.V84I variant registered as SNP (rs34830702) was expressed similarly to the WT. The p.Q431L variant found in a normal control was expressed in a similar pattern but weakly compared to the WT. Exposure time for EGFP and DsRed capture was fixed, enabling direct comparison between different samples. (**B**) Immunoblot analysis of mutant STXBP1 proteins by using a monoclonal Munc18 antibody (top). Upper and lower bands represent EGFP-STXBP1 and endogenous STXBP1 proteins, respectively. Expression of four mutant STXBP1 proteins was not detected, whereas WT and two normal variants could be detected. The observed differences in expression were not due to either transfection or loading differences, because the level of Flag-DsRed was similar in all cases (bottom). Mock, no transfection.


tonic seizures in EIEE and myoclonic seizures in EME. However, EIEE and EME have common features, and it is often difficult to distinguish between them. These three subjects can be diagnosed as EME when myoclonic seizures dominate. Therefore, it is possible that *STXBP1* could be also causative for EME. In terms of genotype–phenotype relationship, we found no difference in clinical data between seven subjects with missense mutations and seven subjects with microdeletion, premature termination codon, or splicing mutations. This finding is supported by our experimental data that both missense mutations and a splicing mutation resulted in haploinsufficiency of *STXBP1*: degradation of STXBP1 proteins with missense mutations and NMD associated with an aberrant splicing.

Recently, Hamdan et al. (2009) reported that two de novo *STXBP1* mutations, p.R388X and c.169 + 1G>A, were identified in 2 of 95 individuals with mental retardation and nonsyndromic epilepsy (2%), suggesting that clinical spectrum of *STXBP1* mutations may be broader. However, it is clear that EIEE is the core phenotype of *STXBP1* aberrations in this Japanese cohort as one-third of EIEE cases harbored its mutations. It is also noteworthy that none of West syndrome cases possessed *STXBP1* mutation, suggesting that subjects with initial West syndrome is rarely caused or not caused by *STXBP1* abnormality.

How haploinsufficiency of *STXBP1* leads to infantile epileptic encephalopathy remains to be elucidated. *STXBP1* abnormalities suggest a novel story in which impaired synaptic vesicle release is involved in pathogenesis of epilepsy. Although no seizures have been reported in *Stxbp1* heterozygous knockout mice (Verhage et al., 2000), they showed impaired synaptic function due to reduced size and

replenishment rate of readily releasable vesicles (Toonen et al., 2006), suggesting that heterozygous deletion of *Stxbp1* indeed affected synaptic function in mice. It is possible that the absence of seizures in *Stxbp1* heterozygous knockout mice might be due to the different genetic background. Because *Stxbp1* mutants have been backcrossed for at least six generations to a C57BL/6 background (Toonen et al., 2006), it would be interesting to examine whether seizures would occur in other genetic background. Alternatively, effect of gene dosage alterations of *STXBP1/Stxbp1* may vary between humans and mice: Humans might be more susceptible than mice; therefore, loss of function of one allele could cause seizures only in humans but not in mice. Appropriate mice models by neatly manipulating gene dosage of *Stxbp1* may mimic human phenotype and enable detailed analysis of pathogenesis of infantile epileptic encephalopathy in relation to impaired synaptic function.

## Acknowledgments

We would like to thank patients and their families for their participation in this study. We would like to thank Dr. Sean Megason for the pCIR vector. This work was supported by Research Grants from the Ministry of Health, Labour and Welfare (N.M. and M.K.), Grant-in-Aid for Scientific Research on Priority Areas-(Research on Pathomechanisms of Brain disorder)-from the Ministry of Education, Culture, Sports, Science and Technology of Japan (N. M.), Grant-in-Aid for Scientific Research from Japan Society for the Promotion of Science (N.M. and M.K.), Grant-in-Aid for Young Scientist from Japan Society for the Promotion of Science (H.S.), Research Promotion Fund from Yokohama Foundation for Advancement of Medical Science (H.S.), Research Promotion Fund from The Uehara Memorial Foundation (H.S.), Research Grants from the Japan Epilepsy Research Foundation (H.S. and M.K.), Grant for 2009 Strategic Research Project of Yokohama City University (H.S.), and Research Grant from Naito Foundation (N.M.).

## Disclosure

We confirm that we have read the Journal's position on issues involved in ethical publication and affirm that this report is consistent with those guidelines. None of the authors has any conflict of interest to disclose.

## References

Bahi-Buisson N, Nectoux J, Rosas-Vargas H, Milh M, Boddaert N, Girard B, Cances C, Ville D, Afenjar A, Rio M, Heron D, N'Guyen Morel MA, Arzimanoglou A, Philippe C, Jonveaux P, Chelly J, Bienvenu T. (2008) Key clinical features to identify girls with CDKL5 mutations. *Brain* 131:2647–2661.

Ciufo LF, Barclay JW, Burgoyne RD, Morgan A. (2005) Munc18-1 regulates early and late stages of exocytosis via syntaxin-independent protein interactions. *Mol Biol Cell* 16:470–482.

Djukic A, Lado FA, Shinnar S, Moshe SL. (2006) Are early myoclonic encephalopathy (EME) and the Ohtahara syndrome (EIEE) independent of each other? *Epilepsy Res* 70(suppl 1):S68–S76.

Engel J Jr. (2006) Report of the ILAE classification core group. *Epilepsia* 47:1558–1568.

Guerrini R, Moro F, Kato M, Barkovich AJ, Shiihara T, McShane MA, Hurst J, Loi M, Tohyama J, Norci V, Hayasaka K, Kang UJ, Das S, Dobyns WB. (2007) Expansion of the first PolyA tract of ARX causes infantile spasms and status dystonicus. *Neurology* 69:427–433.

Hamdan FF, Piton A, Gauthier J, Lortie A, Dubeau F, Dobrzeniecka S, Spiegelman D, Noreau A, Pellerin S, Cote M, Henrion E, Fombonne E, Mottron L, Marineau C, Drapeau P, Lafreniere RG, Lacaille JC, Rouleau GA, Michaud JL. (2009) De novo STXBP1 mutations in mental retardation and nonsyndromic epilepsy. *Ann Neurol* 65: 748–753.

Kalscheuer VM, Tao J, Donnelly A, Hollway G, Schwinger E, Kubart S, Menzel C, Hoeltzenbein M, Tommerup N, Eyre H, Harbord M, Haan E, Sutherland GR, Ropers HH, Gecz J. (2003) Disruption of the serine/threonine kinase 9 gene causes severe X-linked infantile spasms and mental retardation. *Am J Hum Genet* 72:1401–1411.

Kato M, Das S, Petras K, Sawaishi Y, Dobyns WB. (2003) Polyalanine expansion of ARX associated with cryptogenic West syndrome. *Neurology* 61:267–268.

Kato M. (2006) A new paradigm for West syndrome based on molecular and cell biology. *Epilepsy Res* 70(suppl 1):S87–S95.

Kato M, Saitoh S, Kamei A, Shiraishi H, Ueda Y, Akasaka M, Tohyama J, Akasaka N, Hayasaka K. (2007) A longer polyalanine expansion mutation in the ARX gene causes early infantile epileptic encephalopathy with suppression-burst pattern (Ohtahara syndrome). *Am J Hum Genet* 81:361–366.

Maquat LE, Kinniburgh AJ, Rachmilewitz EA, Ross J. (1981) Unstable beta-globin mRNA in mRNA-deficient beta o thalassemia. *Cell* 27:543–553.

Ohtahara S, Ishida T, Oka E, Yamatogi Y, Inoue H, Karita S, Ohtsuka Y. (1976) [On the specific age dependent epileptic syndrome: the early-infantile epileptic encephalopathy with suppression-burst.]. *No to Hattatsu* 8:270–279.

Ohtahara S, Yamatogi Y. (2006) Ohtahara syndrome: with special reference to its developmental aspects for differentiating from early myoclonic encephalopathy. *Epilepsy Res* 70(suppl 1):S58–S67.

Saitsu H, Kato M, Mizuguchi T, Hamada K, Osaka H, Tohyama J, Uruno K, Kumada S, Nishiyama K, Nishimura A, Okada I, Yoshimura Y, Hirai S, Kumada T, Hayasaka K, Fukuda A, Ogata K, Matsumoto N. (2008) *De novo* mutations in the gene encoding STXBP1 (MUNC18-1) cause early infantile epileptic encephalopathy. *Nat Genet* 40:782–788.

Shyu AB, Wilkinson MF, van Hoof A. (2008) Messenger RNA regulation: to translate or to degrade. *EMBO J* 27:471–481.

Stromme P, Mangelsdorf ME, Shaw MA, Lower KM, Lewis SM, Bruyere H, Lutcherath V, Gedeon AK, Wallace RH, Scheffer IE, Turner G, Partington M, Frints SG, Fryns JP, Sutherland GR, Mulley JC, Gecz J. (2002) Mutations in the human ortholog of Aristaless cause X-linked mental retardation and epilepsy. *Nat Genet* 30:441–445.

Toonen RF, Wierda K, Sons MS, de Wit H, Cornelisse LN, Brussaard A, Plomp JJ, Verhage M. (2006) Munc18-1 expression levels control synapse recovery by regulating readily releasable pool size. *Proc Natl Acad Sci U S A* 103:18332–18337.

Verhage M, Maia AS, Plomp JJ, Brussaard AB, Heeroma JH, Vermeer H, Toonen RF, Hammer RE, van den Berg TK, Missler M, Geuze HJ, Sudhof TC. (2000) Synaptic assembly of the brain in the absence of neurotransmitter secretion. *Science* 287:864–869.

Weaving LS, Christodoulou J, Williamson SL, Friend KL, McKenzie OL, Archer H, Evans J, Clarke A, Pelka GJ, Tam PP, Watson C, Lahooti H, Ellaway CJ, Bennetts B, Leonard H, Gecz J. (2004) Mutations of CDKL5 cause a severe neurodevelopmental disorder with infantile spasms and mental retardation. *Am J Hum Genet* 75: 1079–1093.

Yamatogi Y, Ohtahara S. (2002) Early-infantile epileptic encephalopathy with suppression-bursts, Ohtahara syndrome; its overview referring to our 16 cases. *Brain Dev* 24:13–23.

## Supporting Information

Additional Supporting Information may be found in the online version of this article:

**Table S1.** PCR conditions and primer sequences.

Please note: Wiley-Blackwell is not responsible for the content or functionality of any supporting materials supplied by the authors. Any queries (other than missing material) should be directed to the corresponding author for the article.

# Disrupted *SOX10* Regulation of *GJC2* Transcription Causes Pelizaeus-Merzbacher-Like Disease

Hitoshi Osaka, MD, PhD,[1,2]
Haruka Hamanoue, MD, PhD,[3]
Ryoko Yamamoto, MSc,[4]
Atsuo Nezu, MD, PhD,[5] Megumi Sasaki, BA,[4]
Hirotomo Saitsu, MD, PhD,[3]
Kenji Kurosawa, MD, PhD,[6]
Hiroko Shimbo, MP,[1]
Naomichi Matsumoto, MD, PhD,[3]
and Ken Inoue, MD, PhD[4]

Mutations in the gap junction protein gamma-2 gene, *GJC2*, cause a central hypomyelinating disorder; Pelizaeus-Merzbacher-like disease (PMLD; MIM311601). Using a homozygosity mapping and positional candidate gene approach, we identified a homozygous mutation (c.-167A>G) within the *GJC2* promoter at a potent SOX10 binding site in a patient with mild PMLD. Functionally, this mutation completely abolished the SOX10 binding and attenuated *GJC2* promoter activity. These findings suggest not only that the *SOX10*-to-*GJC2* transcriptional dysregulation is a cause of PMLD, but also that *GJC2* may be in part responsible for the central hypomyelination caused by *SOX10* mutations.

ANN NEUROL 2010;68:250–254

Congenital hypomyelinating disorders are a heterogeneous group of central nerve system (CNS) leukoencephalopathies, most of which are inherited disorders of myelin formation. The prototype condition is Pelizaeus-Merzbacher disease (PMD; MIM312080), an X-linked disorder caused by mutations in the proteolipid protein 1 gene (*PLP1*).[1] Patients with PMD have nystagmus, impaired motor development, ataxia, choreoathetotic movements, dysarthria, and progressive spasticity. However, ~20 to 50 % of patients clinically diagnosed with PMD have no detectable abnormalities in the *PLP1* gene, and some have a distinct disease, Pelizaeus-Merzbacher-like disease (PMLD; MIM311601).

Mutations in the gap junction protein gamma-2 gene (*GJC2*, also known as *Cx47* or *GJA12*) have been reported as a cause of PMLD.[2–8] Twenty-four different mutations (8 frameshift, 10 missence, 5 nonsense, and 1 missense/insertion alterations) have been reported to date, and most if not all result in a loss of channel function.[7,9]

By combining homozygosity mapping and a candidate gene approach, we found a homozygous mutation that disrupts a SOX10 transcriptional activation site in the *GJC2* promoter region in a family showing a mild PMLD phenotype. SOX10 is an high mobility group (HMG) family transcription factor that plays a critical role in peripheral nervous system (PNS) and CNS myelination. In addition, a subset of *SOX10* mutations cause peripheral and central hypomyelination, Waardenburg syndrome, and Hirschsprung disease (PCWH; MIM609136).[10] This study reports the first case of PMLD caused by a mutation in the *GJC2* promoter and suggests that *SOX10* transcriptional regulation of *GJC2* plays a critical role in CNS myelination.

## Patients and Methods

Detailed clinical information of a Japanese female patient with PMLD, who is now 25-years-old, was previously reported.[11] In brief, her healthy parents were second cousins. She had congenital pendular nystagmus as a neonate, but otherwise developed normally and was educated at a normal school. At the age of 10 years, she developed a spastic gait that worsened and made her wheelchair bound by the age of 12 years. Her disease progressed to mild athetosis of the upper limbs and ataxia by age 13 years and dysarthria by age 15 years. She cannot speak and understands only easy commands now. Brain magnetic resonance imaging at age 15 and 20 years showed diffuse hyperintensity of white matter on T2-weighted images with interval progression of brain atrophy (Fig 1). Electrophysiological examinations showed extensive nerve conduction slowing in the CNS, although this was less severe than usually seen in male patients with PMD.[11] Peripheral nerve conduction velocities were nor-

From the [1]Division of Neurology, Clinical Research Institute, Kanagawa Children's Medical Center; [2]Molecular Pathology and Genetics Division, Kanagawa Cancer Center Research Institute; [3]Department of Human Genetics, Yokohama City University Graduate School of Medicine; [4]Department of Mental Retardation and Birth Defect Research, National Institute of Neuroscience, National Center of Neurology and Psychiatry, Kodaira; [5]Division of Pediatric Neurology, Yokohama Ryoiku-iryo Center; and [6]Division of Genetics, Clinical Research Institute, Kanagawa Children's Medical Center, Yokohama, Japan.

Address correspondence to Dr Osaka, Division of Neurology, Clinical Research Institute, Kanagawa Children's Medical Center, Yokohama, 232-855, Japan. E-mail: hosaka@kcmc.jp

Additional Supporting Information can be found in the online version of this article.

Received Dec 29, 2009, and in revised form Jan 29, 2010. Accepted for publication Feb 26, 2010.

Published online in Wiley InterScience (www.interscience.wiley.com). DOI: 10.1002/ana.22022

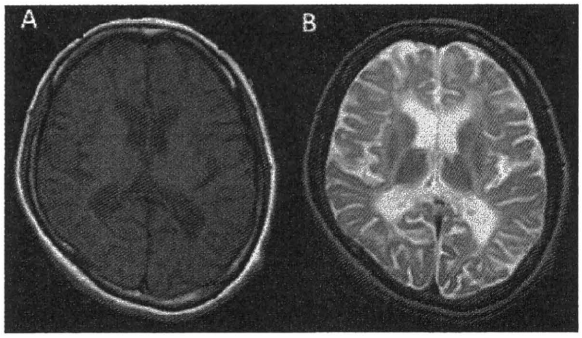


**FIGURE 1: Magnetic resonance imaging of the cerebrum. (A) T1-weighted image of the proband at 20 years shows cerebral atrophy with ventricular dilatation and widening of a subarachnoidal space. Disappearance of contrast between cortex and white matter, which suggested incomplete myelination throughout the cerebrum, was evident. (B) T2-weighted image reveals diffuse hyperintensity in the white matter, suggesting the arrest of myelination. Note that the inner capsule, which is usually myelinated in the neonate, was not myelinated in this patient.**

mal. Molecular examinations excluded *PLP1* exonic mutations, large duplications, and deletions.

Informed consent was obtained from the patient and family members in accordance with human study protocols approved by the institutional review board of Kanagawa Children's Medical Center. Genomic DNA was extracted from peripheral lymphocytes. A genome-wide single nucleotide polymorphism (SNP) genotyping was undertaken for III-1, III-3, IV-1, IV-2, V-1, and V-2 (Fig 2A) using the GeneChip Human Mapping 10K Array *X*ba 142 2.0 (Affymetrix, Santa Clara, CA) containing 10,204 SNPs according to the manufacture's protocols (Supplementary Materials and Methods). Polymerase chain reaction and DNA sequencing are described in the Supplementary Materials and Methods (Supplementary Table 1).

Mammalian cell expression plasmids for the wild-type and E189X mutant human *SOX10* cDNA were reported previously.[12] Luciferase reporter plasmids containing mouse *Gjc2* promoters (kindly provided from Dr M. Wegner) were utilized

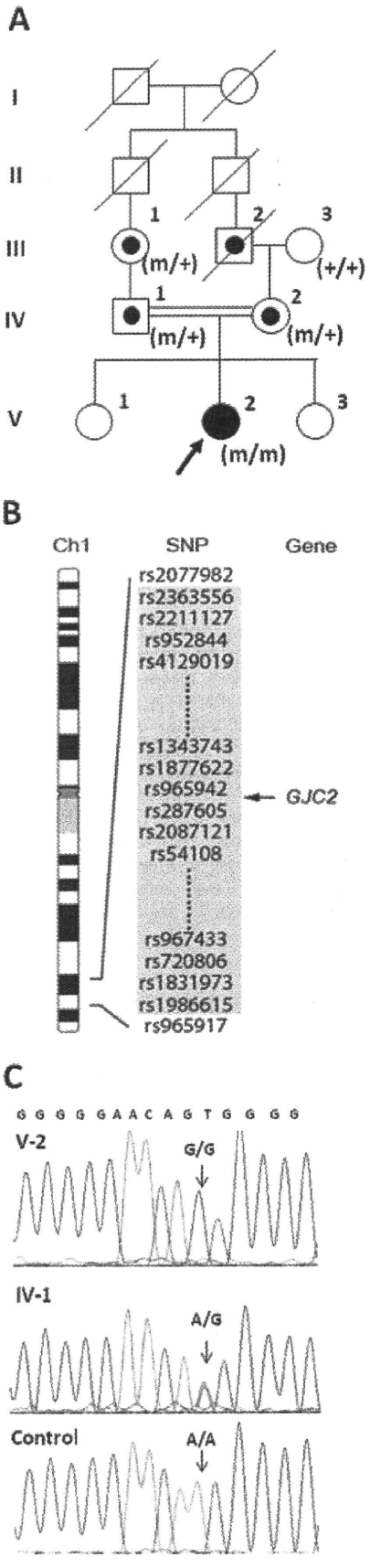


**FIGURE 2: Family pedigree, largest region of interest on chromosome 1, and the *CJC2* mutation. (A) Pedigree of the Pelizaeus-Merzbacher-like disease family with the proband *(filled circle with arrow)*. DNA from III-1, III-3, IV-1, IV-2, V-1, and V-2 were used for single nucleotide polymorphism (SNP) genotyping. Carriers are indicated as circles with black dots. m = mutant allele; + = wild-type allele. (B) The largest region of interest by homozygosity SNP mapping at 1q41-q42.2. The homozygous interval is shown as a shaded square with SNP identifiers. The location of *GJC2* is shown with an arrow. The region between rs2077982 and rs965917 was 18.2 Mb in size (University of California, Santa Cruz genome browser coordinate, chromosome 1: 215150317-233384165, February 2009 version). (C) Sequencing chromatograms from the patient (V-2, top), a carrier (IV-1, middle), and a normal control (bottom). The c.-167A>G mutation in the promoter region of *CJC2* is shown with arrows.**

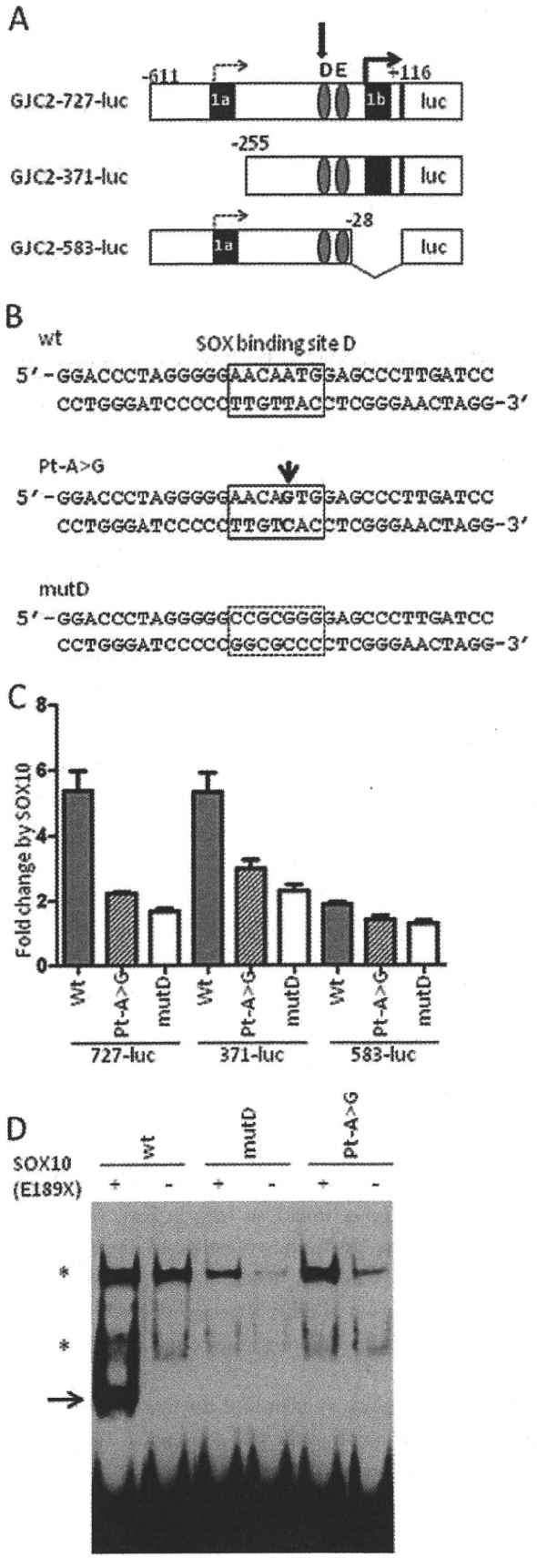


for site-directed mutagenesis (see Supplementary Materials and Methods). We measured *GJC2* transcriptional activity by luciferase reporter assays using human glioblastoma U138 cells (see Supplementary Materials and Methods). SOX10 binding affinity was determined by electrophoretic mobility shift assay (EMSA) using synthetic oligonucleotide probes and nuclear extracts from HeLa cells transfected with pCMV-SOX10-E189X, as previously described.[13]

## Results

The largest region with homozygosity identified by SNP genotyping on chromosome 1q42.13 was our primary focus for candidate gene scanning (see Fig 2B, Supplementary Table 2, Supplementary Fig 1). Among 115 refseq genes mapped within this region, 34 gene products were identified from mouse whole brain proteomics studies (Supplementary Table 3).[14,15] After we sequenced all coding regions and intron-exon boundaries of these 34 genes to exclude any disease-causing mutations, we extended our analysis to promoter regions. We found a homozygous mutation, c.-167A>G, in the proximal promoter re-

**FIGURE 3: Functional consequence of the c.-167A>G point mutation in the *GJC2* promoter. (A) Schematic diagram of the luciferase reporter constructs of mouse *Gjc2* promoter region utilized in this study. Exon 1b contains the major transcription start site *(thick arrow)*, whereas exon 1a contains the minor site *(dotted arrow)*. GJC2-727-luc contains a full proximal promoter, whereas GJC2-371-luc lacks exon 1a and the upstream portion and GJC2-583-luc lacks exon 1b. Two SOX10 binding site, D and E, are shown as shaded ovals with a thick arrow pointing to site D, where the mutation was identified. (B) Sequences of the probes used for electrophoretic mobility shift assays (EMSAs). Top: *wt* probe containing the wild-type site D *(square)*. Middle: Pt-A>G probe carrying c.-167A>G mutation *(arrow)*. Bottom: mutD probe in which site D was changed to abolish SOX10 binding. (C) Transcriptional activities of different *GJC2* promoter constructs carrying either wt, Pt-A>G, or mutD at site D shown as fold changes obtained by presence or absence of SOX10 determined by luciferase reporter assay. Note that the *wt* constructs for 727-luc and 371-luc, harboring the major start site in exon 1b, were activated by SOX10 >5-fold. In contrast, a much smaller effect was observed when either Pt-A>G or mutD was introduced. The 583-luc constructs, which only harbor a minor transcription start site, remain inactivated by SOX10 regardless of changes in site D. Each bar represents average ± standard deviation. Each experiment was performed 3×, each in triplicate. Results from a representative experiment were shown. (D) DNA binding affinity of each probe (shown in B) was determined by EMSA using nuclear extracts from HeLa cells transfected with plasmid expressing truncated SOX10 protein (E189X) or empty plasmid (as a negative control). The *wt* probe showed a strong binding to E189X SOX10 protein, which retains enhanced DNA binding ability *(arrow)*. In contrast, we observed no binding of the mutant probes, either mutD or Pt-A>G. Asterisks show nonspecific binding. Free probes were observed at the bottom of the picture.**

gion of *GJC2* that segregated with PMLD in the family members (see Fig 2A and C) and was absent in 122 normal Japanese chromosomes. Analysis of this region in 10 additional female PMLD patients without mutations in the open reading frame of *GJC2* detected no abnormalities.

Interestingly, this mutation is located within a critical SOX10 binding site (designated as site D) in the syntenic mouse *Gjc2* proximal promoter and diminishes the consensus of the SOX binding sequence (AACAATG to AACAGTG, Fig 3A and B). Based on this, we predicted that this mutation disrupts *GJC2* promoter activity and measured transcription in vitro using a luciferase reporter system. Because the region harboring the mutation is highly conserved across mammals,[16] we introduced this mutation into well-studied mouse *Gjc2* promoter constructs (see Fig 3A and B). The c.-167A>G point mutation in the SOX10 binding site dramatically decreased transcription to levels similar to a completely disrupted SOX10 binding site D (see Fig 3C). These findings suggest that the c.-167A>G point mutation found in our patients results in a diminished *GJC2* transcription.

Based on these results, we hypothesized that this mutation altered SOX10 binding affinity to site D and tested this by EMSA. Because full-length SOX10 has a low binding affinity that is difficult to distinguish from background noise, we used a C-terminus truncation version of SOX10, E189X, which retains the HMG binding domain and has enhanced binding affinity.[16] Introduction of the c.-167A>G mutation into site D resulted in a complete loss of E189X SOX10 binding (see Fig 3D). Therefore, combined with the preceding observations, we find that the c.-167A>G mutation abolishes SOX10 binding to the *GJC2* promoter, resulting in a dramatic attenuation of the *GJC2* transcription.

## Discussion

*GJC2* encodes Cx47, a member of the connexin family. Connexins are components of gap junctions, intercellular channels that allow ions and small molecules to pass across neighboring plasma membranes. Gap junctions have diverse functions, including the propagation of electrical signals and metabolic cooperation. Two hemichannels, each built up of 6 connexin protein subunits on opposing cell membranes, form the channel. Astrocytes and oligodendrocytes are coupled by gap junctions constructed predominantly of GJC2 (Cx47) and Cx43.[17] Because Cx47 proteins carrying PMLD-causing mutations either fail to reach the membrane or have reduced transport activity, loss of function is likely the mechanism underlying the CNS hypomyelination in PMLD.[7,9] Herein we report the first *GJC2* promoter mutation,[18] c.-167A>G, in a patient with PMLD, and this is associated with allelic transcription failure.

Our female patient had nystagmus, spasticity, and choreoathetosis, clinical symptoms common to PMD and PMDL. However, she attained normal motor and intellectual developmental milestones. Because only $\frac{1}{3}$ (11 of 33) of PMLD patients with *GJC2* mutations have walked unsupported,[2–7] her clinical manifestation was mild and overlaps with that of spastic paraplegia phenotype. Of note, she lost her motor and cognitive abilities within a few years, accompanied by progressive brain atrophy (see Fig 1). Such acute regression has rarely been observed in PMD and is more characteristic of PMLD secondary to *GJC2* mutations.[6]

A recent study showed that SOX10 directly regulates *GJC2* by binding to its proximal promoter.[16] Site D, the SOX10 binding site in which our mutation was identified, plays a predominant role in *GJC2* promoter activity,[16] and the c.-167A>G mutation we identified reduces its affinity for SOX10 and abolishes *GJC2* transcription. These findings suggest that *SOX10* regulation of *GJC2* via site D is essential for proper *GJC2* expression and that its failure causes PMLD. Presumably, the relatively milder clinical phenotype observed in our patient results from reduced but not completely abolished transcriptional activity, allowing translation of a small amount of normal Cx47 protein.

This constitutes the second disorder associated with dysregulation of a SOX10 target gene. Previously, mutations within the *SOX10* binding site of the *GJB1* promoter have been shown to cause demyelinating peripheral neuropathy.

Together the peripheral neuropathy and PMLD provide a partial understanding of the clinical manifestations of PCWH patients. Because these patients have SOX10 mutations,[10] we predict that the expression of both *GJC2* and *GJB1* is impaired. Impaired expression of both of these genes would, at least in part, respectively account for the de-/hypomyelination of the CNS and PNS observed in PCWH. Based on this, we predict that impaired expression of other target genes of SOX10 is responsible for the Hirschprung disease and other Waardenburg features.

In conclusion, we identified the first case of PMLD caused by a mutation in the *GJC2* promoter. Because this mutation disrupts SOX10 regulation of *GJC2* transcription, we hypothesize that SOX10 regulation of transcription plays a major role in nervous system myelination.

## Acknowledgments

This study was supported by grants-in-aid for scientific research from the Ministry of Education, Culture, Sports, Science, and Technology, Japan (H.O., K.I.), Takeda Science Foundation (H.O.), Yokohama Foundation for Advancement of Medical Science (H.O.), and Kanagawa children's hospital (K.K., H.O.), and Health Labor Sciences Research Grants from the Ministry of Health, Labor, and Welfare, Japan (H.O., K.K., N.M., K.I.).

We thank Dr M. Wegner for kindly providing us plasmid DNAs and Drs C. Boerkoel, C. du Souich, and P. Atkins for their critical reviews.

## Potential Conflicts of Interest

Nothing to report.

## References

1. Inoue K. PLP1-related inherited dysmyelinating disorders: Pelizaeus-Merzbacher disease and spastic paraplegia type 2. Neurogenetics 2005;6:1–16.
2. Uhlenberg B, Schuelke M, Ruschendorf F et al. Mutations in the gene encoding gap junction protein alpha 12 (connexin 46.6) cause Pelizaeus-Merzbacher-like disease. Am J Hum Genet. 2004;75:251–260.
3. Bugiani M, Al Shahwan S, Lamantea E et al. GJA12 mutations in children with recessive hypomyelinating leukoencephalopathy. Neurology. 2006;67:273-279.
4. Wolf NI, Cundall M, Rutland P et al. Frameshift mutation in GJA12 leading to nystagmus, spastic ataxia and CNS dys-/demyelination. Neurogenetics. 2007;8:39–44.
5. Salviati L, Trevisson E, Baldoin MC et al. A novel deletion in the GJA12 gene causes Pelizaeus-Merzbacher-like disease. Neurogenetics. 2007;8:57-60.
6. Henneke M, Combes P, Diekmann S et al. GJA12 mutations are a rare cause of Pelizaeus-Merzbacher-like disease. Neurology. 2008;70:748-754.
7. Orthmann-Murphy JL, Salsano E, Abrams CK et al. Hereditary spastic paraplegia is a novel phenotype for GJA12/GJC2 mutations. Brain. 2009;132:426–438.
8. Wang J, Wang H, Wang Y et al. Two novel gap junction protein alpha 12 gene mutations in two Chinese patients with Pelizaeus-Merzbacher-like disease. Brain Dev. 2009; doi:10.1016/j.braindev.2009.03.013.
9. Orthmann-Murphy JL, Enriquez AD, Abrams CK, Scherer SS. Loss-of-function GJA12/Connexin47 mutations cause Pelizaeus-Merzbacher-like disease. Mol Cell Neurosci. 2007;34:629–641.
10. Pingault V, Bondurand N, Kuhlbrodt K et al. SOX10 mutations in patients with Waardenburg-Hirschsprung disease. Nat Genet. 1998;18:171-173.
11. Nezu A, Kimura S, Uehara S et al. Pelizaeus-Merzbacher-like disease: female case report. Brain Dev. 1996;18:114–118.
12. Inoue K, Khajavi M, Ohyama T et al. Molecular mechanisms for distinct neurological phenotypes conveyed by allelic truncating mutations. Nat Genet. 2004;36:361–369.
13. Inoue K, Ohyama T, Sakuragi Y et al. Translation of SOX10 3' untranslated region causes a complex severe neurocristopathy by generation of a deleterious functional domain. Hum Mol Genet. 2007;16:3037–3046.
14. Taylor CM, Marta CB, Claycomb RJ et al. Proteomic mapping provides powerful insights into functional myelin biology. Proc Natl Acad Sci U S A. 2004;101:4643–4648.
15. Wang H, Qian WJ, Chin MH et al. Characterization of the mouse brain proteome using global proteomic analysis complemented with cysteinyl-peptide enrichment. J Proteome Res. 2006;5:361–369.
16. Schlierf B, Werner T, Glaser G, Wegner M. Expression of connexin47 in oligodendrocytes in regulated by the Sox10 transcription factor. J Mol Biol. 2006;361:11–21.
17. Orthmann-Murphy JL, Freidin M, Fischer E et al. Two distinct heterotypic channels mediate gap junction coupling between astrocyte and oligodendrocyte connexins. J Neurosci. 2007;27:13949–13957.
18. Ruf N, Uhlenberg B. Analysis of human alternative first exons and copy number variation of the GJA12 gene in patients with Pelizaeus-Merzbacher-like disease. Am J Med Genet B Neuropsychiatr Genet. 2009;150B:226–232.
19. Bondurand N, Girard M, Pingault V et al. Human Connexin 32, a gap junction protein altered in the X-linked form of Charcot-Marie-Tooth disease, is directly regulated by the transcription factor SOX10. Hum Mol Genet. 2001;10:2783-2795.
20. Houlden H, Girard M, Cockerell C et al. Connexin 32 promoter P2 mutations: a mechanism of peripheral nerve dysfunction. Ann Neurol. 2004;56:730–734.

RESEARCH ARTICLE

Human Mutation

OFFICIAL JOURNAL
HGVS
HUMAN GENOME VARIATION SOCIETY
www.hgvs.org

# Loss-of-Function Mutations of *CHST14* in a New Type of Ehlers-Danlos Syndrome

Noriko Miyake,[1*†] Tomoki Kosho,[2†] Shuji Mizumoto,[3†] Tatsuya Furuichi,[4] Atsushi Hatamochi,[5] Yoji Nagashima,[6] Eiichi Arai,[7] Kazuo Takahashi,[8] Rie Kawamura,[2] Keiko Wakui,[2] Jun Takahashi,[9] Hiroyuki Kato,[9] Hiroshi Yasui,[10] Tadao Ishida,[10] Hirofumi Ohashi,[11] Gen Nishimura,[12] Masaaki Shiina,[13] Hirotomo Saitsu,[1] Yoshinori Tsurusaki,[1] Hiroshi Doi,[1] Yoshimitsu Fukushima,[2] Shiro Ikegawa,[4] Shuhei Yamada,[3] Kazuyuki Sugahara,[3] and Naomichi Matsumoto[1*]

*[1]Department of Human Genetics, Yokohama City University Graduate School of Medicine, Yokohama, Japan; [2]Department of Medical Genetics, Shinshu University School of Medicine, Matsumoto, Japan; [3]Laboratory of Proteoglycan Signaling and Therapeutics, Hokkaido University Graduate School of Life Science, Sapporo, Japan; [4]Laboratory for Bone and Joint Disease, Center for Genomic Medicine, RIKEN, Tokyo, Japan; [5]Department of Dermatology, Dokkyo Medical University, School of Medicine, Tochigi, Japan; [6]Department of Molecular Pathology, Yokohama City University Graduate School of Medicine, Yokohama, Japan; [7]Department of Pathology, Saitama Medical University, Saitama, Japan; [8]Department of Environmental Immuno-Dermatology, Yokohama City University Graduate School of Medicine, Yokohama, Japan; [9]Department of Orthopedics, Shinshu University School of Medicine, Matsumoto, Japan; [10]First Department of Internal Medicine, Sapporo Medical University, Sapporo, Japan; [11]Division of Medical Genetics, Saitama Children's Medical Center, Saitama, Japan; [12]Department of Radiology, Tokyo Metropolitan Kiyose Children's Hospital, Tokyo, Japan; [13]Department of Biochemistry, Yokohama City University Graduate School of Medicine, Yokohama, Japan*

Communicated by Jürgen Horst

Received 17 March 2010; accepted revised manuscript 24 May 2010.
Published online 8 June 2010 in Wiley InterScience (www.interscience.wiley.com). DOI 10.1002/humu.21300

**ABSTRACT:** Ehlers-Danlos syndrome (EDS) is a heterogeneous connective tissue disorder involving skin and joint laxity and tissue fragility. A new type of EDS, similar to kyphoscoliosis type but without lysyl hydroxylase deficiency, has been investigated. We have identified a homozygous *CHST14* (carbohydrate sulfotransferase 14) mutation in the two familial cases and compound heterozygous mutations in four sporadic cases. *CHST14* encodes dermatan 4-*O*-sulfotransferase 1 (D4ST1), which transfers active sulfate from 3′-phosphoadenosine 5′-phosphosulfate to position 4 of the *N*-acetyl-D-galactosamine (GalNAc) residues of dermatan sulfate (DS). Transfection experiments of mutants and enzyme assays using fibroblast lysates of patients showed the loss of D4ST1 activity. *CHST14* mutations altered the glycosaminoglycan (GAG) components in patients' fibroblasts. Interestingly, DS of decorin proteoglycan, a key regulator of collagen fibril assembly, was completely lost and replaced by chondroitin sulfate (CS) in the patients' fibroblasts, leading to decreased flexibility of GAG chains. The loss of the decorin DS proteoglycan due to *CHST14* mutations may preclude proper collagen bundle formation or maintenance of collagen bundles while the sizes and shapes of collagen fibrils are unchanged as observed in the patients' dermal tissues. These findings indicate the important role of decorin DS in the extracellular matrix and a novel pathomechanism in EDS.
Hum Mutat 31:966–974, 2010. © 2010 Wiley-Liss, Inc.

**KEY WORDS:** Ehlers-Danlos syndrome; EDS; *CHST14*; dermatan sulfate; dermatan 4-*O*-sulfotransferase 1; D4ST1; collagen bundle formation; decorin

## Introduction

Ehlers-Danlos syndrome (EDS) is a heterogeneous connective tissue disorder characterized by joint and skin laxity and tissue fragility [Steinmann et al., 2002], affecting as many as 1 in 5,000 individuals. The pathomechanisms of EDS consist of dominant-negative effects of mutant procollagen α-chains, α-chain haploinsufficiency, and deficiency of collagen-processing enzymes [Mao and Bristow, 2001]. In a revised nosology [Beighton et al., 1998], EDS was classified into six major types as well as additional minor forms. We previously described two unrelated patients showing characteristic facial and skeletal features with partial similarity to kyphoscoliosis type EDS but without lysyl hydroxylase deficiency (EDS-VIB) [Kosho et al., 2005]. Through long-term clinical evaluation of them as well as additional four unrelated patients including one reported previously [Yasui et al., 2003], we confirmed that these patients represent a new type of EDS [Kosho et al., 2010]. The evidence that two of six probands were born between consanguineous parents (Fig. 1A) suggests that this disease is inherited in an autosomal recessive fashion. Thus, we performed homozygosity mapping to find the disease-causative gene and successfully identified pathological mutations in the carbohydrate sulfotransferase 14 (*CHST14*: GenBank reference sequence, NM_130468.3) gene, in all six probands. *CHST14* encodes dermatan 4-*O*-sulfotransferase 1 (D4ST1), which transfers active sulfate to the *N*-acetyl-D-galactosamine (GalNAc) residues of dermatan sulfate (DS). Furthermore, we

Additional Supporting Information may be found in the online version of this article.

†The first three authors contributed equally to this article.

*Correspondence to: Noriko Miyake, Department of Human Genetics, Yokohama City University Graduate School of Medicine, 3-9 Fukuura, Kanazawa-ku, Yokohama 236-0004, Japan. E-mail: nmiyake@yokohama-cu.ac.jp or Naomichi Matsumoto, Department of Human Genetics, Yokohama City University Graduate School of Medicine, 3-9 Fukuura, Kanazawa-ku, Yokohama 236-0004, Japan. E-mail: naomat@yokohama-cu.ac.jp

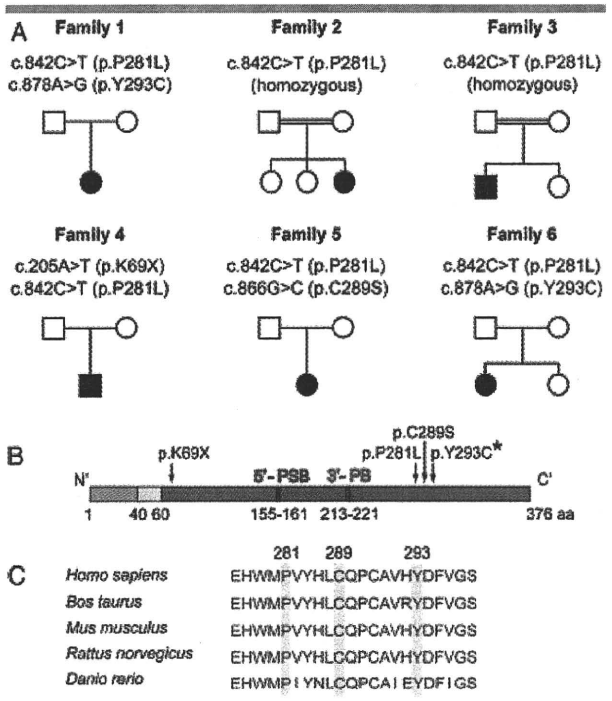


**Figure 1.** *CHST14* mutations in the patients. **A:** Pedigrees of the patients. Mutations in both alleles were found in all. **B:** A schematic representation of D4ST1 encoded by *CHST14*. Arrows indicate the position of mutations found in the patients. The red and blue boxes indicate a 5′-phosphosulfate binding site (5′-PSB) and a 3′-phosphate binding site (3′-PB), respectively. Light blue, yellow, and purple boxes denote cytoplasmic, transmembrane, and luminal regions, respectively. *p.Y293C (c.878A>G) is the same missense mutation identified in the Japanese ATCS sibs reported [Dündar et al., 2009]. **C:** D4ST1 amino acid alignment for three missense mutations evolutionally conserved.

conducted pathological and glycobiological investigations to reveal the pathomechanism of this disease.

## Materials and Methods

### Subjects

We analyzed six Japanese patients clinically diagnosed as showing a specific type of EDS [Kosho et al., 2005, 2010] in this study. Briefly, they clinically resemble the kyphoscoliosis type EDS characterized by joint laxity, progressive scoliosis, tissue fragility with atrophic scars, easy bruising, arterial rupture, and Marfanoid habitus. However, the lysyl hydroxylase deficiency, which is the reliable diagnostic test for the kyphoscoliosis type, was not observed in the probands [Kosho et al., 2005, 2010]. One of the authors (T.K.) evaluated all cases. This study was approved by the institutional review boards of Yokohama City University School of Medicine, Shinshu University School of Medicine, and Hokkaido University Graduate School of Advanced Life Science. Informed consent was obtained from all subjects involved in this study.

### Mapping and Mutation Analysis

We performed the whole genome linkage analysis using Affymetrix Human Mapping single nucleotide polymorphism (SNP) 10K XbaI 142 2.0 array (Affymetrix, St. Clara, CA) in two affected probands (patients 2 and 3) and six unaffected members from two consanguineous families. Haplotype analysis was performed using seven microsatellite markers (*D15S1002, D15S1007, D15S118, D15S1044, D15S214, D15S978,* and *D15S117*) purchased from Applied Biosystems (Bedford, MA). These markers were designed based on the Marshfield genetic map (http://research.marshfieldclinic.org/genetics). We screened three affected individuals (patients 1, 2, and 3) for mutations in seven genes (*THBS1, FSIP1, VSP39, MEIS2, DLL4, CHAC1,* and *CHST14*) among 109 known genes within the 7.3-Mb candidate locus. After identifying a mutation, we only screened *CHST14* (NM_130468.3) in the remaining individuals (patients 4, 5, and 6). We amplified genomic DNA by PCR using four primer sets (sequences available on request). Nucleotide changes found in the patients were checked in 376 Japanese control samples (752 alleles). Compound heterozygosity was confirmed by direct sequencing of the patients' parents or allele specific sequencing after cloning of respective regions covering two different mutation sites of *CHST14*. Nucleotide numbering reflects cDNA numbering with +1 corresponding to the A of the ATG translation initiation codon in the reference sequence, according to journal guidelines (www.hgvs.org/mutnomen). The initiation codon is codon 1.

### Primary Fibroblast Culture

We obtained skin fibroblasts from patient 1 at age 6 years, her mother at 27 years, and patient 3 at 29 years. Their age- and sex-adjusted normal controls (a 6-year-old girl: control 1 and a 36-year-old man: control 2) were purchased from Japan Health Sciences Foundation (http://www.jhsf.or.jp/). Cells were cultured in Dulbecco's modified Eagle's medium with 10% heat-inactivated fetal bovine serum (FBS), 100 U/ml penicillin, 100 U/ml streptomycin, and 2 mM L-glutamine (Invitrogen, Carlsbad, CA).

### Sulfotransferase Assays

COS-7 cells transiently transfected with the N′-V5-D4ST1 vectors using FuGENE™ 6 (Roche Diagnostics, Indianapolis, IN) and human fibroblasts were lysed with 200 µl of M-PER® mammalian protein extraction reagent (Thermo Fisher Scientific Inc., Waltham, MA). Sulfotransferase activities of each cell lysate toward dermatan, chemically desulfated DS were assayed as described before [Mikami et al., 2003]. The [$^{35}$S]sulfate incorporation was quantified by determination of the radioactivity in the flow-through fractions of the gel filtration chromatography by liquid scintillation counting.

### Disaccharide Composition Analysis of Chondroitin (CS)/DS Chains Isolated from Fibroblasts

Cell lysates of fibroblasts cultured on 100-mm plates were digested with actinase E (Kaken Pharmaceutical Co., Ltd., Tokyo, Japan) and GAG-peptides were recovered by 80% ethanol as described [Uyama et al., 2006]. After being desalted using a centrifugal filter, Amicon® Ultra-4 (Ultracel-3k, Millipore Corp., Billerica, MA), the GAG-peptides were digested with CSase ABC from *Proteus vulgaris* (EC 4.2.2.20) (Seikagaku Corp., Tokyo, Japan) [Yamagata et al., 1968], a mixture of CSase AC-I from *Flavobacterium heparinum* (EC 4.2.2.5) (Seikagaku Corp.) [Yamagata et al., 1968], and AC-II from *Arthrobacter aurescens* (EC 4.2.2.5) (Seikagaku Corp.) [Hiyama and Okada, 1975], or CSase B from *Flavobacterium heparinum* (EC 4.2.2.19) (IBEX Technologies, Kawasaki, Japan) [Michelacci and Dietrich, 1974]. The digests were labeled with a fluorophore 2-aminobenzamide (2AB) and aliquots

of the 2AB-derivatives of CS/DS oligosaccharides were analyzed by anion-exchange HPLC on a PA-03 column (YMC Co., Kyoto, Japan) as previously described [Kinoshita and Sugahara, 1999].

### Immunoblotting

Each cell lysate of COS-7 cells expressing the recombinant N′-V5-D4ST1 was subjected to SDS-PAGE using a 10–20% SDS-polyacrylamide gradient gel. The serum-free conditioned medium from fibroblast cultures was collected and concentrated using Amicon Ultra-4 filters (Ultracel-30k). An aliquot of the sample was digested with CSase ABC, CSase AC, CSase B, or buffer alone, and each digest was subjected to SDS-PAGE using a 7.5% SDS-polyacrylamide gel. Immunoblotting was carried out using anti-V5 antibody (Invitrogen) for D4ST1-transfected cells or antihuman decorin antibody (clone 115402; R&D Systems, Minneapolis, MN) for secreted decorin DS proteoglycan from fibroblasts.

### PAI1 and SMAD7 Expression Analysis with TGF-β1 Stimulation

Fibroblasts were grown to 70–80% confluence in 24-well multiplates and transfected with 200 ng of empty, wild-type, or mutant *CHST14* expression vector, using FuGENE 6. At 24 hr after transfection, cells were transferred to low serum medium (0.2% FBS) and, after 8 hr treated with TGF-β1 (1 ng/ml; PeproTech Inc., Rocky Hill, NJ) for 24 hr. Total RNA was extracted using the SV-Total RNA Isolation system (Promega, Madison, WI). Randomly primed cDNA was synthesized using the Taqman Multiscribe Reverse Transcriptase kit (Applied Biosystems). Real-time PCR was carried out on the StepOnePlus Real-Time PCR system (Applied Biosystems) using the QuantiTect SYBR Green PCR kit (Qiagen, Tokyo, Japan). The following primers were used for amplification: *CHST14*, 5′-CTATGA-GAGGCTGGAGGCTG-3′ and 5′-AGGCAAAGAGGGAGAAGTCC-3′; *PAI1*, 5′-CAGACCAAGAGCCTCTCCAC3′ and 5′- GACTGTTCC-TGTGGGGTTGT-3′; *SMAD7*, 5′-TTGCTGTGAATCTTACGGGA-3′ and 5′-CCAGATAATTCGTTCCCCCT-3′; and *GAPDH*, 5′-ACCA-CAGTCCATGCCATCAC-3′ and 5′-TCCACCACCCTGTTGCTGTA-3′.

### Reporter Gene Assay

Fibroblasts were grown to 70–80% confluence in 24-well multiplates and transfected with plasmid DNA mixtures using FuGENE 6. The DNA mixture involved 100 ng of SBE4-luc vector, 200 ng of empty, wild-type, or mutant *CHST14* expression vector, and 25 ng of a reference vector, pRL-TK. The SBE4-Luc vector is a TGF-β-responsive reporter containing four tandem copies of a SMAD-binding element (SBE) linked to luciferase [Zawel et al., 1998]. At 24 hr after transfection, cells were transferred to low serum medium (0.2% FBS) and, after 8 hr, treated with TGF-β1 (1 ng/ml) for a further 24 hr. Luciferase activities were measured using the PG-DUAL-SP reporter assay system (Toyo Ink., Tokyo, Japan) and a Lumat LB 9507 luminometer (Berthold Technologies GmbH & Co. KG, Bad Wildbad, Germany). Relative luciferase activity was calculated by normalizing the transfection efficiency of Renilla luciferase activity against the reference vector.

### SMAD2 Phosphorylation with TGF-β1 Stimulation

Fibroblasts were grown to 70–80% confluence in six-well multiplates and were transfected with 1.5 μg of empty, wild-type, or mutant *CHST14* expression vector, using FuGENE 6. At 24 hr after transfection, cells was transferred to low serum medium (0.2% FBS) and, after 8 hr, were treated with TGF-β1 (1 ng/ml) for 30 min. Cells were lysed using M-PER protein extraction kits (Pierce, Rockford, IL) containing a protease inhibitor cocktail (Roche Diagnostics). Proteins in the cell lysate were separated on SDS-PAGE gels and electrophoretically transferred to PVDF membranes. After blocking with 5% nonfat dry milk in PBS-Tween, the membranes were incubated first with antibodies against phospho-SMAD2 or SMAD2 (Cell Signaling Technology, Danvers, MA) and then with goat polyclonal antibodies against rabbit IgG conjugated with horseradish peroxidase (Cell Signaling Technology). Band intensities were measured using ImageJ software (http://rsbweb.nih.gov/ij/).

### Pathology

Skin specimens were obtained from the upper arms of patients 5 and 6. For light microscopy using a BX51 microscope (Olympus, Tokyo, Japan), skin specimens were fixed with 20% buffered neutral formalin solution and 3–5-μm sections were stained with H&E. For transmission electron microscopy, skin specimens were fixed in 2.5% glutaraldehyde for 2 hr, postfixed in 1% osmium tetroxide for 2 hr, dehydrated in a graded ethanol series, and embedded in epoxy resin (Epon 812, TAAB, Berks, UK). Semithin sections (4 μm) were stained with toluidine blue. Ultrathin sections (100 nm) were stained with uranyl acetate and lead citrate and examined with a transmission electron microscope (JEM-1011, JEOL Ltd., Tokyo, Japan).

### Statistical Analyses

All values are described as mean ± SEM. Where appropriate, we assessed between-groups effects by unpaired *t* tests for two groups and ANOVA with Dunnett's adjustment for more than two groups using GraphPad Prism 5 for Windows, version 5.02 (www.graphpad.com).

The detailed methods are described in the Supp. Methods.

## Results

### Genetic Analysis

We performed homozygosity mapping of two independent consanguineous families (families 2 and 3) and identified the largest 8.15-Mb homozygous region at chromosome 15q14–q15.3 with the maximum LOD Score 2.885, and by using additional microsatellite markers narrowed it down to a 7.3-Mb region (Supp. Fig. S1). Among 109 known genes within this region, the *CHST14* gene (encoding D4ST1) harbored the same homozygous missense mutation (c.842C>T: p.P281L) in the two families and compound heterozygous mutations in the other four (Fig. 1A and B). Mutations include one nonsense (c.205A>T: p.K69X) and three missense mutations (c.842C>T: p.P281L, c.866G>C: p.C289S, and c.878A>G: p.Y293C) occurring at evolutionally conserved amino acids (Fig. 1C). They were absent in 376 Japanese normal controls.

### Sulfotransferase Activity

D4ST1 transfers a sulfate group from 3′-phosphoadenosine 5′-phosphosulfate to position 4 of the *N*-acetyl-D-galactosamine (GalNAc) residues of DS, which is abundantly expressed in skin, aortic wall, tendon, and bone [Penc et al., 1998]. Mutant D4ST1 proteins showed significantly decreased sulfotransferase activity towards dermatan (Fig. 2A) regardless of similar expression levels (Fig. 2B). The sulfotransferase activity was also measured in the